Chapter IV

Plasmonic Nanomaterial Based Electrochemical Sensing

CHAPTER IV
PLASMONIC NANOMATERIAL BASED ELECTROCHEMICAL SENSING

- *The study emphasizes on fabrication of electrochemical schemes for detecting milk adulterants.*
- *Functionalised nanoparticles (NPs) drop casted on glass coated with indium tin oxide (ITO) were used as working electrodes.*
- *APTES-coated, green tea-reduced gold nanoparticles (AuNPs) were deposited onto an ITO electrode were used for urea detection, with cyclic voltammetry (CV) showing increased oxidation peaks with rising urea concentration in milk supernatant.*
- *Similarly, melamine was detected using poly ethylene glycol (PEG)-coated, maleic acid (MA)-functionalized silver nanoparticles (AgNPs) on an ITO electrode, where rise in oxidation peak current was observed with rise in concentration of melamine in milk supernatant.*
- *Hydrogen peroxide was sensed using polyvinyl pyrrolidone (PVP)-functionalized AgNPs coated ITO glass slides, with CV graph showing increased reduction peaks with rising hydrogen peroxide concentration in milk supernatant.*
- *Calibration plots determined detection limits and sensitivity. For urea, melamine and hydrogen peroxide, the limit of detection (LOD) value was found to be 4.02 ppm, 12.24 ppb and 5.19 ppb, respectively.*

4.1 Introduction

Plasmonic nanomaterials (NMs) have emerged as powerful tools in the field of electrochemical sensing, owing to their unique optical and electronic characteristics. These materials exhibit localized surface plasmon resonance (LSPR) when interacting with light at specific wavelengths, leading to enhanced electromagnetic fields at their surfaces [1]. This phenomenon provides exceptional sensitivity in detecting various analytes, especially when integrated with electrochemical techniques [2]. Plasmonic NMs-based electrochemical sensors enable high precision in monitoring small molecular interactions, even at low concentrations, making them suitable for applications in environmental applications, biomedical diagnostics, and food safety monitoring [3]. By combining the

high sensitivity and precision of electrochemical transduction with the signal amplification from plasmonic effects, plasmonic NPs-modified sensors offer enhanced sensitivity, improved selectivity, and remarkable versatility compared to conventional methods [4,5].

These NSs are implemented as electrochemical sensors through integration with electrode materials to exploit their signal-enhancing properties. These structures, often AgNPs or AuNPs, are deposited onto electrode surfaces, when a target analyte binds on the NPs surface, the LSPR effect amplifies the electric field around the NSs, increasing the sensitivity of the electrochemical signal [6]. By combining plasmonic materials with electrochemical techniques, researchers achieve higher sensitivity and lower LOD compared to traditional sensors. Furthermore, the tunability of NSs shape, size, and composition allows for tailored sensor designs that can selectively target various analytes [7,8].

Milk adulteration poses serious health risks and has become a significant concern in the dairy sector [9]. Conventional testing methods often require extensive preparation and laboratory analysis, limiting their use for rapid or on-site detection. Electrochemical sensing, enhanced by plasmonic NSs, offers a promising alternative due to its good selectivity, heightened sensitivity, and potential for real-time monitoring [10]. When applied to milk adulterant detection, these sensors can detect common adulterants—such as urea, melamine and hydrogen peroxide—at low concentrations. The combination of plasmonic enhancement with electrochemical techniques is thus revolutionizing quality control in the dairy industry [11,12].

4.2 Materials and methods

Fresh cow milk was procured from a local milk vendor. Processed green tea (GT) leaves were procured from Tezpur University market, Assam, India. Banana root bulb (BRB) was obtained from the nearby village area of Tezpur, Napaam, Assam, India. Silver Nitrate ($AgNO_3$) was purchased from Thermo Fisher Scientific. Choloroauric acid Trihydrate ($HauCl_4.3H_2O$) was purchased from HiMedia. (3-Aminopropyl)-triethoxysilane (≥98.0%) (APTES), maleic acid (MA), poly vinyl pyrrolidone (PVP), polyetheylene glycol (PEG), trisodium citrate (TSC), sodium borohydride ($NaBH_4$) and sodium hydroxide (NaOH) were purchased from Merck, USA.

Acetone, methanol, and ethanol obtained from Qualigens and were utilised for cleaning purpose. Microscopic glass substrate procured from a local surgical store was used for characterisation purpose. Indium Tin Oxide (ITO) coated glass slides were obtained from Macwin, India. All glass wares and magnetic stirrers used in synthesis were dipped in freshly prepared aqua regia (HNO_3: HCl; 1:3) overnight and rinsed in distilled water (DW) and preserved until dry.

4.3 Instrumentation

A UV−Visible spectrophotometer (Thermo Scientific GENESYS 180); an X-ray powder diffractometer (XRD) (D8 FOCUS, Bruker AXS, GERMANY& BRUKER D8 ADVANCE ECO); a Transmission electron microscope (TEM) (Tecnai G2 20 S-TWIN, USA); a Field emission scanning electron microscope (FESEM) (JEOL & GEMINI 500); a potentiostat for cyclic voltametric studies (OrigaFlex - OGF05A); a weighing machine (METTLER TOLEDO ME204); a centrifuge machine (Eppendorf 5430R); an oven (Ecogian series; EQUITRON); a tabletop pH meter (EUTECH pH 700), and a magnetic stirrer (SPINOT-TARSONS) were also used during the work.

4.4 Electrochemical sensing of urea

Milk is a vital source of essential nutrients, meeting substantial daily requirements for energy, protein, and calcium. Its high nutritional value fuels constant demand, but this popularity also makes milk vulnerable to adulteration [13,14]. Raw cow milk naturally contains about 87% water and 13% solids, where the solid content includes fat and solids-not-fat (SNF) components like proteins, carbohydrates, and minerals such as calcium. Adulteration often begins by diluting milk with water or milk whey, which is then followed by the addition of other substances to mimic natural composition and quality indicators [15,16].

A prominent adulterant in milk is urea, with high nitrogen content that is sometimes fraudulently added to falsify the net protein content. Because many protein tests rely on nitrogen as a measure of protein, suppliers add urea to simulate a higher protein level [17,18].

Urea is inexpensive and readily available, making it a convenient yet illegal addition to milk that increases its perceived quality and market value. However, elevated levels of urea—above the FSSAI limit of 700 ppm—pose significant health risks [19]. Over time, high urea intake can lead to kidney damage as the kidneys have to work harder to eliminate nitrogenous waste, consequently resulting in renal impairment. This is especially dangerous for children, who can experience gastrointestinal distress, nausea, diarrhoea, and even chronic conditions with prolonged exposure [20,21].

Thus, detection of urea in milk is crucial. Traditional methods such as gas chromatography (GC), high-performance liquid chromatography (HPLC), and other techniques like the para-dimethylaminobenzaldehyde (DMAB) test can accurately detect urea but often involve time-consuming preparation steps, high costs, and skilled operators [22]. To address these limitations, there is growing interest in developing rapid, user-friendly, and cost-effective detection methods [23].

Biosensors offer promising solutions for urea detection, overcoming the disadvantages of traditional methods [24]. Urease-based biosensors, which utilize the enzyme's specificity for urea, include electrochemical, optical, and colorimetric techniques. These biosensors are not only efficient but also allow for portability and faster results [25]. Recent advances in nanotechnology also highlight the potential of NP-based sensors, which utilize unique optical properties of NPs for detecting urea and other adulterants [26-28].

Conventionally colorimetric assays and LSPR based methods are useful; however, they come with limitations. Colorimetric methods, while user-friendly, can lack sensitivity and quantitative accuracy, and LSPR, although highly sensitive, often requires complex instrumentation and precise control of particle size for reliable results [29].

On the other hand, electrochemical detection presents a promising alternative for urea detection in milk. This approach leverages electrochemical sensors that convert urea concentration into measurable electrical signals [30]. Electrochemical sensors for urea detection are typically based on enzymes like urease, which catalyses the urea hydrolysis which converts it into carbon dioxide and ammonia, creating a pH change that can be

detected through a variety of electrochemical techniques such as amperometry, potentiometry, or conductometry [31]. These methods are highly sensitive, allowing for accurate quantitative measurements of urea even at low concentrations. Additionally, electrochemical sensors offer several advantages over colorimetric and LSPR methods, including faster response times, and higher sensitivity [32].

In line with this, several studies have focused on the detection of urea using appropriate electrochemical methods, as demonstrated by different research groups. Magar *et al.* fabricated a screen-printed electrodes (SPE) coated with Copper Oxide/Cobalt Oxide on Multi-Walled Carbon Nanotubes (CuO/Co_3O_4@MWCNTs) for non-enzymatic electrochemical sensing of urea with LOD of 0.223 pM [33]. Liu *et al.,* fabricated a portable platform for urea sensing by using AgNPs deposited commercial glucose test strip. They observed a linear working range of 1–8 mM with a LOD of 0.14 mM [34]. In another work, Sharma *et al.* fabricated Titanium Dioxide-Lignin-Loaded Silver Nanoparticles (TiO_2-LL@AgNPs) where the AgNPs were synthesised with *Leucaena leucocephala* leaf extracts. The nanocomposite was used for detection of urea in milk. The range of sensing was between 5.0 µM - 25.0 µM, with a sensitivity of 5.0 mV μM^{-1} cm^{-2}, and LOD of 2.48 µM [35]. While these electrochemical sensors have shown promise in the detection of urea in milk, they are associated with certain disadvantages. Firstly, these electrochemical sensors require complex fabrication processes involving NMs or composite coatings, which can increase production costs and limit scalability for widespread commercial applications. Another disadvantage lies in the sensitivity and specificity of these sensors when exposed to complex sample matrices like milk, which can lead to sensor degradation.

In this work, a non-enzymatic based electrochemical detector has been presented specifically designed for sensing urea in milk. Recognizing the need for a reliable, cost-effective, and easy-to-fabricate detection method, a sensor is developed utilizing APTES-coated AuNPs. AuNPs were chosen for their excellent conductivity, stability, and compatibility with biological matrices. The APTES coating not only stabilizes the AuNPs but also enhances the sensor's interaction with urea molecules by providing a functionalized surface that can improve sensitivity and selectivity.

Unlike enzyme-based sensors, non-enzymatic approach addresses limitations related to enzyme stability, response time, and operational cost, which are often challenging in the dairy industry's complex milk matrices. The electrochemical route also offers a rapid and accurate platform for detecting urea without requiring intricate sample preparation, making it highly suitable for real-time, on-site monitoring.

4.4.1 Synthesis of APTES coated *Camellia sinensis* reduced AuNPs and pretreatment of milk

Preparation of Green Tea Extract: A 100 mL beaker containing 50 mL of DW was heated for 10 min. Afterward, 3 g of dried GT leaves were added to the heated water, and the mixture was further heated for another 10 min to release antioxidants from the leaves. The extract was then double-filtered using Whatman filter paper no. 1 and stored at 4^{o}C for future use [36].

Preparation of AuNPs: A 50 mL beaker containing 20 mL of 1 mM $HAuCl_4.3H_2O$ solution was heated to 70°C for 15 min under constant stirring at 600 rpm. Then, 400 µL of green tea extract was added, and the mixture was further heated until the solution turned wine red, indicating NP formation. The pH was adjusted to 7 using NaOH, and the NPs were incubated at 50^{o}C for 2 h [36].

Pretreatment of milk: Same protocol was implemented as outlined in the previous study (section 2.A.1.1). After following this process, the resultant milk supernatant, was then spiked with various concentrations of urea (10 to 150 ppm) for subsequent testing

4.4.2 Characterisation of APTES coated *Camellia sinensis* reduced AuNPs

UV-Vis spectroscopy was performed to analyse the absorption spectra of the synthesized NPs. An intense broad absorption spectrum was obtained starting from 450 to 600 nm, with a maximum at 530 nm as shown in **Fig. 4.1.a** [37].

XRD study displayed four distinct peaks were observed at 38.18°, 44.38°, 64.64°, and 77.83°, corresponding to the (111), (200), (220), and (311) diffraction planes, respectively.

The presence of these characteristic diffraction peaks confirms that the synthesized AuNPs exhibit a face-centred Cubic (FCC) crystalline structure (**Fig. 4.1.b**) [38].

TEM analysis revealed the shape and size of the NPs. Particle synthesised were of sizes spanning between 4 and 20 nm, while the average diameter measured approximately 12.09 nm. Moreover, the morphological examination depicted a predominantly spherical configuration (**Fig. 4.1.c; Fig. 4.1.d & Fig. 4.1.e**) [39]. Similarly, the FESEM examination yielded compelling insights, revealing that the NPs exhibited a primarily spherical morphology (**Fig. 4.1.f**) [40].

The cyclic voltammetry (CV) analysis of the fabricated electrode APTES/AuNP/APTES/ITO was measured between - 1.0 to 1.0 V at 100 mV/s in 0.1 M phosphate saline buffer (PBS) (pH = 7.2), which acted as electrolyte. During the positive sweep or negative sweep of the CV, no significant peak can be observed asserting no prominent oxidation or reduction in absence of the analyte (**Fig. 4.1.g**) [41].

4.4.3 Electrochemical sensing

4.4.3.1 Fabrication of the sensor

The ITO glass substrate (1 cm × 2 cm) was prepared by sequential cleaning. Initially, it was immersed in methanol and DW, followed by 30 min of sonication, and then rinsed five times with DW to remove any residual methanol. This was followed by another immersion in DW with an additional 30 min of sonication. The cleaned substrate was then dried by heating in an oven at 80°C for 15 min.

The dry ITO glass was then immersed in a 1% APTES solution at 60°C for 1 h. After this, the substrate was thoroughly washed to remove any unbound APTES from the surface. Next, 500 µL of AuNPs was drop-cast onto the APTES-treated ITO glass substrate, a process repeated four times to enhance deposition. The coated substrate was sintered at 100°C to ensure uniform NPs coverage. Finally, a 0.5% APTES layer was applied by drop-casting 200 µL of APTES onto the AuNP-coated ITO glass slides, followed by sintering at 80°C for 2 h to secure the final coating (**Fig. 4.2**) [42,43].

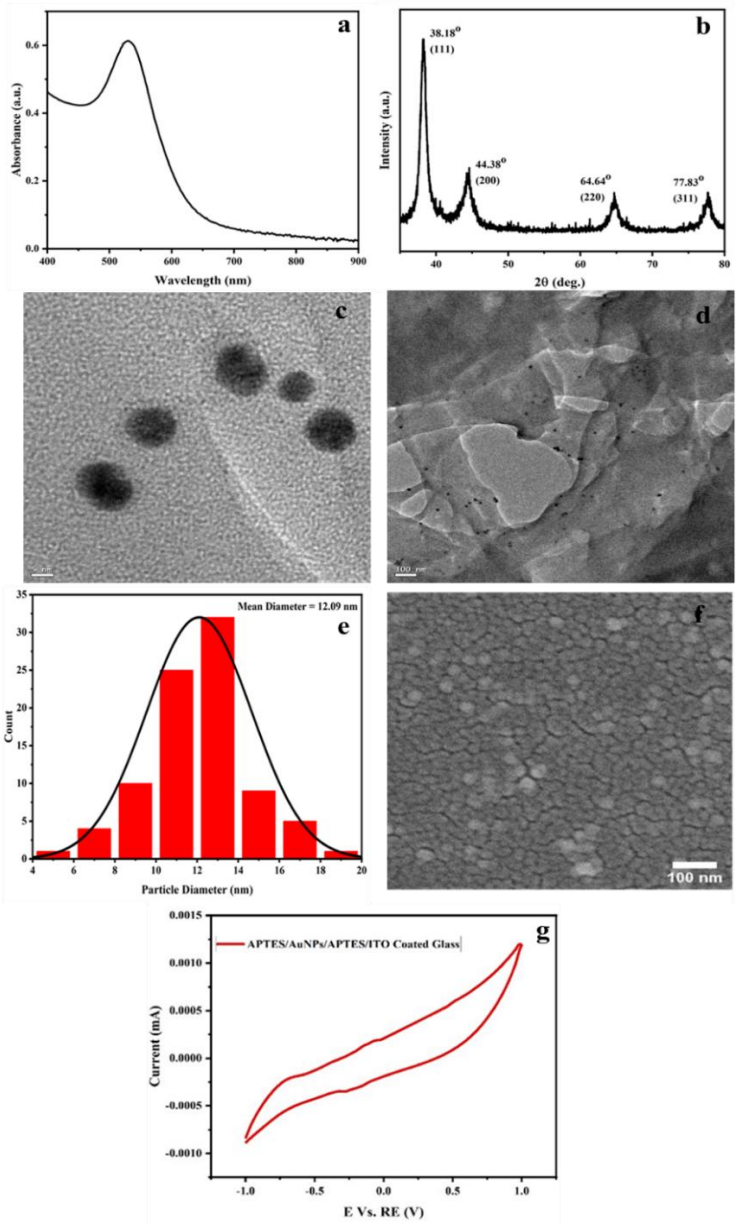

***Figure 4.1**: Characterisation of APTES/AuNPs, **(a)** UV-Vis absorbance spectrum, **(b)** XRD pattern, **(c)** TEM image (under high magnification), **(d)** TEM image (under low magnification), **(e)** size distribution analysis from TEM, **(f)** FESEM image, and (g) cyclic voltametric analysis.*

4.4.3.2 Preliminary investigation of the working electrode

To verify the successful formation and electroactivity of the modified electrode, a ferricyanide test was conducted, commonly used to confirm the electrochemical reactivity of electrodes, particularly the working electrode. In this test, 5 mM potassium ferricyanide in 0.4 M KCl was used as the electrolyte. The fabricated electrode demonstrated increased oxidation and reduction peaks, comparable to those seen in ferricyanide/ferrocyanide

conversion, indicating enhanced electrochemical reactivity and conductivity. This response suggests that the modified electrode, with its APTES/AuNPs/APTES coating, has favourable electron transfer properties, essential for effective electrochemical detection [44].

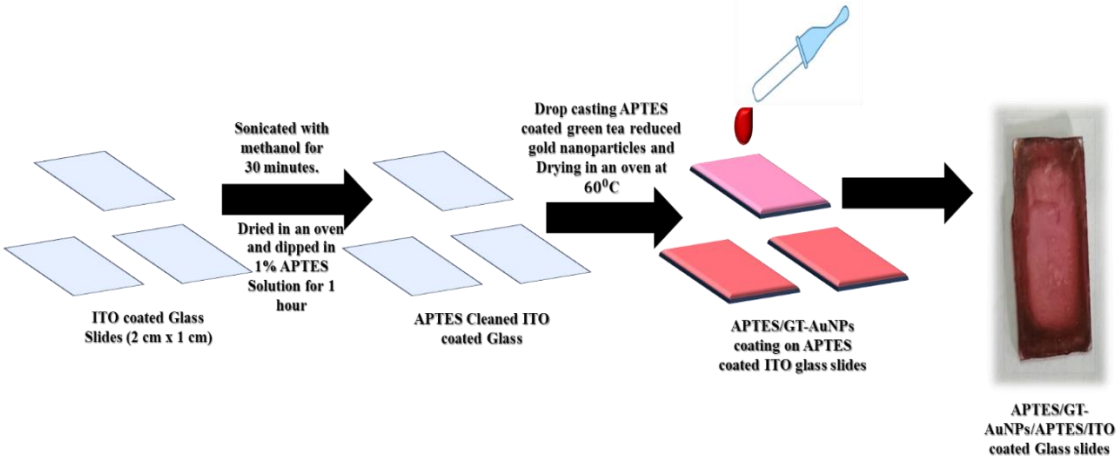

Figure 4.2: *Schematic illustration of fabrication of APTES/GT-AuNPs/APTES/ITO coated glass slides as a working electrode.*

4.4.3.3 Mechanism

In this electrochemical sensing setup, AuNPs were deposited onto an ITO electrode, significantly increasing the surface area available for electrocatalytic activity. The electrode was then immersed in a slightly alkaline solution containing urea and a supporting electrolyte, such as phosphate-buffered saline at pH 8.5, which maintains optimal conditions for urea detection. The ITO electrode serves as the conductive substrate, while an APTES layer ensures strong adhesion of the AuNPs to the ITO surface. The AuNPs, in turn, provide catalytic sites that enhance electron transfer and enable direct electrochemical oxidation of urea without the need for enzymes like urease [44-47].

During the detection process, the modified electrode, functionalized with APTES and loaded with AuNPs, interacts with urea molecules. The amine groups ($-NH_2$) on APTES facilitate the adsorption of urea onto the electrode surface through hydrogen bonding and electrostatic interactions (at slightly alkaline pH). This adsorption allows urea to accumulate at the electrode surface, where it undergoes electrochemical oxidation when a potential is applied. The oxidation process generates products such as carbon dioxide (CO_2) and nitrogen (N_2), producing a measurable oxidation current. The AuNPs act as efficient catalytic agents, reducing the oxidation potential and enhancing the current

response. This results in a distinct and pronounced oxidation peak in the voltammogram, enabling sensitive detection of urea [44].

This oxidation peak, having a direct correlation with urea concentration, provides a quantitative measure of urea in the solution. Successive additions of urea lead to systematic increment in the peak current, demonstrating the sensor's high sensitivity and rapid response, with steady-state signals achieved within seconds. The cyclic voltametric response shows no significant peaks in the potential window of -1.0 V to 1.0 V vs. Ag/AgCl in the absence of urea, while clear oxidation peaks appear upon urea addition, confirming effective urea detection. This process is highly reproducible and stable, avoiding the instability associated with enzyme-based systems.

The sensitivity of this detection process is pH-dependent, as protonation of urea's $-NH_2$ group at lower pH inhibits interaction with the AuNPs, reducing the sensor's efficacy. For optimal results, the sensor is maintained at slightly basic pH, such as 8.5, where the interaction between urea and AuNPs is maximized, enabling accurate and sensitive urea detection [48]. The oxidation of urea occurs in three steps.

Adsorption: The APTES layer, with its amine groups interacts with urea molecules through hydrogen bonding or electrostatic interactions. This causes urea molecules to concentrate near the AuNPs on the electrode surface (Reaction 4.1).

$$CO(NH_2)_2 + APTES \rightarrow [APTES\cdots CO(NH_2)_2] \quad (\mathbf{4.1})$$

Catalytic Oxidation: AuNPs then facilitate the electron transfer required for urea oxidation, enhancing the rate of electron transfer during the oxidation of urea (Reaction 4.2) [48].

$$[APTES\cdots CO(NH_2)_2] + 6OH^- \xrightarrow{AuNPs} CO_2 + N_2 + 5H_2O + 6e^- \quad (\mathbf{4.2})$$

Electron Transfer to Electrode: The six electrons released during urea oxidation are transferred through the AuNPs to the ITO electrode, generating an oxidation current that is detected by the electrochemical sensor [44,47-49].

4.4.3.4 Sensor performance metrics

The modified working electrode was further assessed for non-enzymatic urea detection using cyclic voltammetry. For these measurements, the electrode setup included an APTES/AuNPs/APTES ITO-coated glass slide as the working electrode, an Ag/AgCl electrode as the reference, and platinum as the counter electrode, with 0.2 M PBS and 0.4 M KCl at pH 8.5 as supporting electrolytes. The effective surface area of the working electrode was approximately 1 cm^2, and measurements were conducted over a potential range from -1.0 V to 1.0 V. In the absence of urea, no significant peak was observed. However, upon adding urea, a prominent oxidation peak appeared, accompanied by a smaller reduction peak.

The reduction peak observed in the cyclic voltammetry analysis in the presence of urea is attributed to the electrochemical reduction of intermediate products formed during the urea oxidation process. While urea oxidation is typically an irreversible reaction, certain electroactive intermediates generated during this process can participate in secondary redox reactions. The reduction peak corresponds to these intermediates returning to a lower oxidation state, producing a cathodic (reduction) peak in the CV curve. This redox cycling highlights the electrode's catalytic activity and stability, demonstrating its ability to facilitate secondary reversible reactions, which are crucial for enhancing sensitivity and reliability in urea detection [50,51].

The oxidation peak current increased with higher concentrations of urea in the milk supernatant, demonstrating a positive correlation between urea concentration and current response [44]. To evaluate the selectivity of the electrode, a bare electrode was used as a control (**Fig. 4.3**). The absence of any significant oxidation peak in this case confirmed the high selectivity of the APTES/AuNPs/APTES-coated electrode for urea detection, likely due to the catalytic effect of the AuNPs. This observation implies that the modified electrode’s specific design enhances its sensitivity to urea, while unmodified electrodes fail to generate detectable urea signals [44,48].

The oxidation peak observed near 0.4 V in the presence of urea is attributed to the oxidation reaction facilitated by the APTES/AuNPs on the electrode surface (**Fig 4.4**). A calibration curve of peak oxidation current vs. urea concentration was plotted, yielding

a linear increase with a regression coefficient (R^2) of 0.97. Using this calibration graph, the LOD was determined using equation 2.1 which was found to be 4.02 ppm, and the sensitivity was calculated to be 7.46×10^{-4} mA/ppm. The recovery rate was found to be between 95.05%- 99.44%, which was calculated using equation 2.2 and error associated with the sensor was also calculated as reported in **Table 4.1**. Compared to other sensors, this modified electrode offers a simpler and more robust approach for detecting urea, even in trace amounts below permissible limits (**Fig 4.5**) [44].

The reproducibility of the sensor was assessed by measuring peak current responses across different electrodes with identical urea concentrations, demonstrating consistent peak currents and reliability (**Fig. 4.6.a**). Reusability was confirmed by conducting multiple cycles with the same electrode and analysing the resulting CV responses, showing stable performance (**Fig. 4.6.b**). To further evaluate the stability, electrodes were stored in a vacuum to prevent oxidation and tested over a period of 5 days. CV measurements at intervals indicated that the electrodes-maintained functionality for urea detection with minor variability, suggesting a viable shelf life. This performance stability over time supports the potential for commercializing the sensor for practical urea detection applications (**Fig. 4.6.c**) [44,48,52].

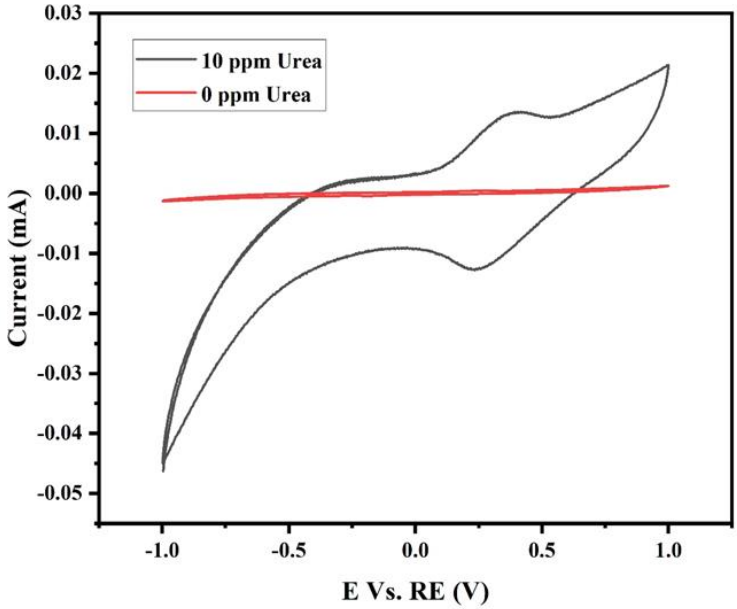

Figure 4.3: *Sensing performance of the APTES/AuNPs/APTES ITO electrode in absence and presence of urea (Reference Electrode: Ag/AgCl; Auxiliary Electrode: Pt; Electrolyte: 0.2 M PBS and 0.4 M KCl at pH 8.5; Scan rate: 0.1 V/sec).*

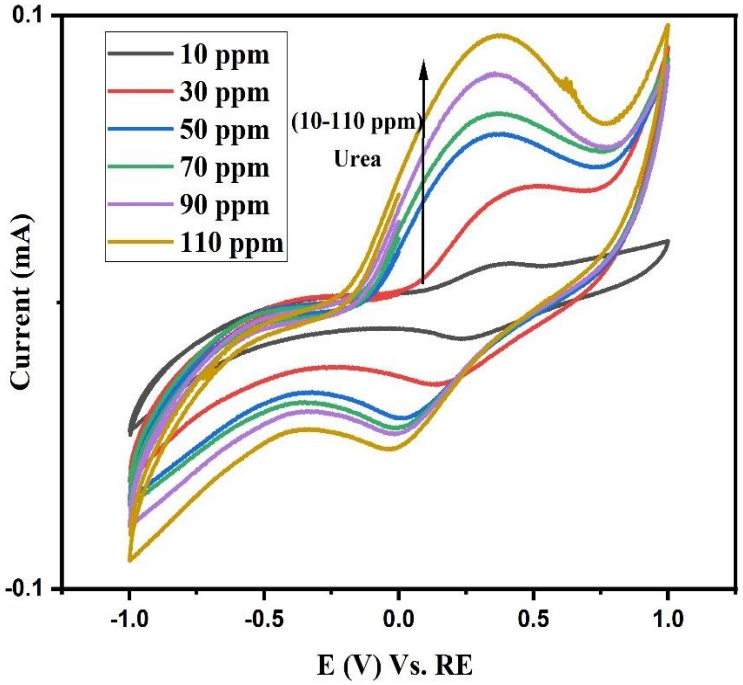

Figure 4.4: *CV Analysis of ITO electrode system fabricated with APTES/AuNPs/APTES coated ITO electrode in presence of different concentration of urea in milk supernatant (Reference Electrode: Ag/AgCl; Auxiliary Electrode: Pt; Electrolyte: 0.2 M PBS and 0.4 M KCl at pH 8.5; Scan rate: 0.1 V/sec).*

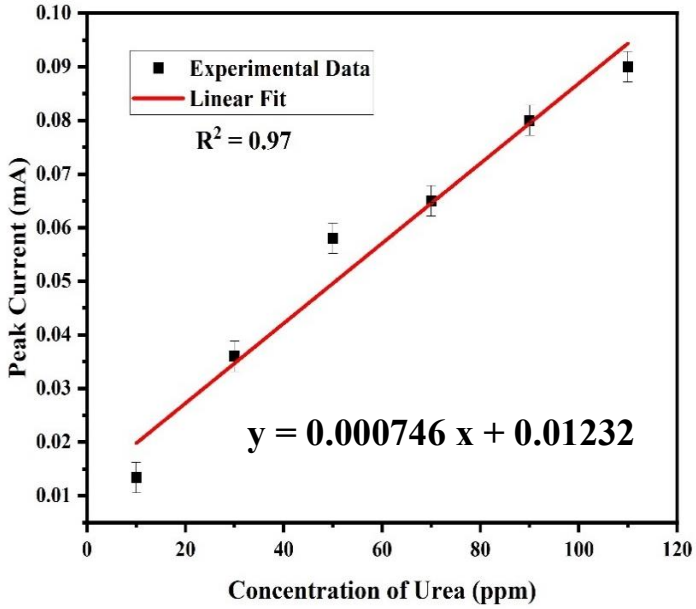

Figure 4.5: *Calibration graph plotted between maximum oxidation current vs. the increase in concentration of urea in milk supernatant.*

Table 4.1: *Quantitative estimation of urea in milk.*

Sl. no.	Peak current (mA)	Theoretical value of concentration (x_0) (ppm)	Experimental value of concentration (x) (ppm)	Error % $(\frac{x_0 - x}{x_0} \times 100)$
1	0.0265	20	19.01	4.95
2	0.0418	40	39.52	1.2
3	0.0555	60	57.88	3.5
4	0.0713	80	79.06	1.18
5	0.0865	100	99.44	0.56

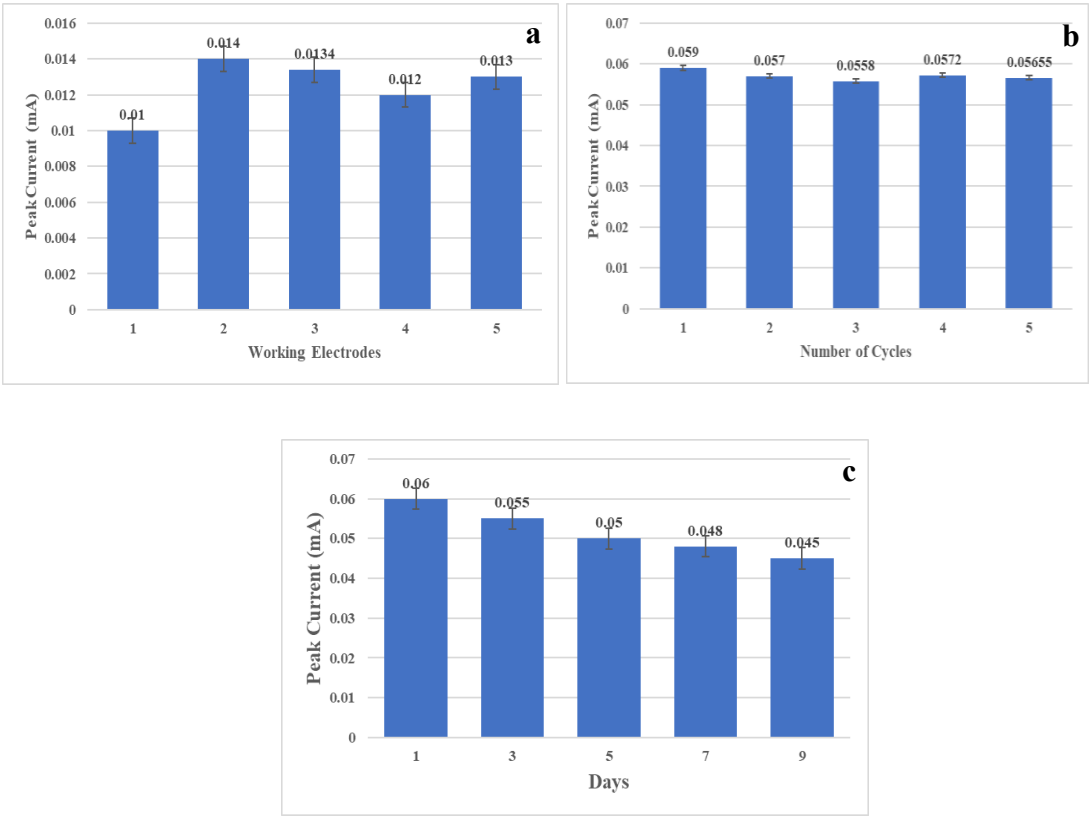

Figure 4.6: *CV response of the electrochemical sensor in the presence of urea* ***(a)*** *with different electrodes,* ***(b)*** *different cycles with the same electrode, and* ***(c)*** *with electrode stored at different times (Electrolyte: 0.2 M PBS; Scan rate: 100 mV/s).*

4.5 Electrochemical sensing of melamine

Melamine is a nitrogen rich organic compound commonly utilised in the production of resins, plastics, and other industrial materials [53]. However, it has also been used in several food contamination scandals. Particularly, it is unlawfully added to milk and dairy products to artificially inflate the protein content by increasing the content of nitrogen in milk [54]. High levels of melamine consumption pose significant health risks, including kidney damage, urinary tract infections, and, in severe cases, kidney stones or failure. These incidents underscore the reliable solution, for highly sensitive, and selective methods to detect melamine at trace levels in milk samples [55,56].

Although traditional analytical methods for melamine detection provide high sensitivity and specificity [57-60], however, they are often expensive requiring sophisticated instrumentation, skilled operators, and long sample preparation process, limiting their application for rapid, on-site screening. In response to these limitations, electrochemical sensing has emerged as a promising alternative for melamine detection, offering a rapid, portable, and easy-to-use solution to detect melamine with high selectivity.

Electrochemical sensing for melamine detection leverages the principles of electrochemical reactions at the electrode surface, where the presence of melamine induces measurable changes in current or potential [61]. This method typically involves modifications to the electrode surface to enhance sensitivity, selectivity, and stability. NMs, such as metal NPs, carbon NSs (e.g., graphene, carbon nanotubes), and conductive polymers, have become central to the development of electrochemical melamine sensors due to their unique electrical, catalytic, and adsorption properties [62,63]. These materials not only enhance the surface area of the working electrode but also facilitate electron transfer, improving the sensor's detection limits and response times [64].

In the case of melamine detection, electrochemical sensors can be engineered to recognize specific molecular interactions. Melamine's structure, featuring multiple nitrogen atoms, makes it a suitable target for electrochemical detection based on interactions with metal ions, conductive polymers, or functionalized NMs that exhibit specific affinities for nitrogen-containing molecules [65].

This interaction can lead to changes in the electrode's electrochemical behaviour, typically observed in CV or differential pulse voltammetry (DPV) studies, where shifts in current peak or potential indicate the presence and concentration of melamine [66,67].

Some studies have reported the sensing of melamine in milk using specially fabricated working electrodes. For instance, Chen *et al.* developed an AuNPs and reduced graphene oxide (rGO) modified electrode to detect melamine. Under optimized conditions, this electrode displayed linearly correlated plot with increase in melamine concentrations between 5.0 to 50 nM [68]. But one disadvantage of this method is the complexity and cost associated with the fabrication of electrodes modified with AuNPs and rGO. These materials and processes require specialized equipment and expertise, which limits accessibility and scalability, especially for routine or on-site testing. Additionally, the sensitivity of this method can be influenced by potential interferences from other compounds present in complex samples like milk, which may affect the accuracy of melamine detection without extensive sample preparation or purification. This complexity makes the method less practical for widespread, rapid testing in resource-limited settings.

To overcome this lacuna, in this work, a novel method has been devised for detecting trace amounts of melamine in complex matrices like milk, using an electrochemical sensor platform based on a PEG and maleic acid-coated AgNPs system on an APTES-modified ITO coated glass slide. This design leverages the unique properties of each component to enhance the sensitivity, selectivity, and stability of the sensor for accurate melamine detection. The PEG/maleic acid coating on AgNPs provides stability to the NPs, reduces nonspecific binding, and introduces functional groups that enable selective interaction with melamine molecules. AgNPs, known for their excellent conductivity and catalytic properties, significantly enhances the electron transfer, which amplifies the sensor signal and enabling detection at low melamine concentrations. Additionally, the maleic acid groups serve as specific binding sites for melamine, facilitating selective capture even in the complex sample matrix of milk. The APTES coating on the ITO glass slide provides a functional, adhesive layer that uniformly binds AgNPs, stabilizing the electrode surface and improving electrochemical performance. This layer increases the sensor's active surface area, enhancing its interaction with melamine ions and contributing to improved sensitivity and detection limits.

The electrode interacts with melamine in milk supernatant by producing a distinct oxidation peak. This peak serves as a measurable signal directly related to the melamine concentration, allowing for accurate detection even at trace levels. The PEG/maleic acid-coated AgNPs/APTES-ITO platform offers a fast, cost-efficient, and highly selective solution for melamine detection without relying on enzymes. This non-enzymatic design reduces the need for expensive equipment and labour-intensive sample preparation, making it ideal for on-site testing.

4.5.1 Synthesis of PEG coated maleic acid functionalised AgNPs and pretreatment of milk

Preparation of reducing and functionalising agents: 10 mM $AgNO_3$ solution was prepared by adding 0.169 g in 100 mL of DW. For uniform dissolution of the precursor salt the solution was stirred at room temperature for a duration of 10 min at a stirring rate of 600 rpm. Following this, 20 mM of $NaBH_4$ solution was prepared by dissolving 0.076 g in 100 mL of DW for a duration of 5 min at room temperature at a stirring rate of 600 rpm. To properly cap and encapsulate the NPs, 1% TSC solution was prepared for which 1 g of TSC was dissolved in 100 mL of DW at room temperature and a stirring rate of 600 rpm. For functionalisation of NPs 0.2 M maleic acid solution was prepared for which 0.42 g of maleic acid was added to 20 mL of DW and stirred at room temperature for a duration of 10 min at a rate of 600 rpm. 0.1 M NaOH solution was prepared to adjust the pH of the solution. For encapsulation, 3 g of PEG was dissolved in 100 ml of DW and stirred for 2 h at room temperature to obtain 3 % PEG solution.

Preparation of functionalised NPs: To prepare the NPs, 28 mL of $NaBH_4$ was continuously stirred at 800 rpm, to it 14 mL of 10 mM $AgNO_3$ solution was added dropwise under continuous stirring. The colour of the solution immediately changed from colourless to yellow to dark yellow colour indicating formation of NPs in the solution. To prevent aggregation of particles, 5 mL of TSC was added to this colloidal solution under continuous stirring at 800 rpm at room temperature. The stirring of NPs was continued for 20 min for uniform encapsulation and capping of each NP by the negatively charged citrate group. Following this 2 mL of 0.2 M maleic acid solution was added to the synthesised NP solution which was then stirred at 900 rpm for 30 min at room temperature for uniform

surface functionalisation of the citrate capped NPs. The pH of the solution was then adjusted to 7 by addition of 0.1 M NaOH solution under continuous stirring at 700 rpm. The resulting solution was deep yellow in colour indicating formation of smaller sized maleic acid functionalised AgNPs. To this solution for proper encapsulation of PEG, 3% PEG solution was added to the colloidal solution of NPs and stirred for 6 h at room temperature resulting in formation of PEG capped maleic acid functionalised AgNPs [69,70].

Pretreatment of milk: Same protocol was implemented as outlined in the previous study (section 2.A.1.1). After following this process, the resultant milk supernatant, was then spiked with various concentrations of melamine (5 to 60 ppb) for subsequent testing

4.5.2 Characterisation of PEG coated maleic acid functionalised AgNPs

Characterisation of the NPs were performed by following the previous protocol (section 4.4.2). UV–Visible analysis displayed an intense broad absorption peak at 391 nm, which corresponds to the LSPR peak of AgNPs (**Fig. 4.7.a**) [71].

To determine the structural characteristics of synthesised NPs, XRD characterisation was performed. Four distinct peaks were observed in the XRD pattern at an angle of 38.41°, 44.74°, 64.75°, and 77.66°, corresponding to the diffraction planes (111), (200), (220), and (311), respectively. The presence of these characteristic diffraction peaks confirms that the synthesized AgNPs exhibit an FCC crystalline structure (**Fig. 4.7.b**) [72].

The size distribution analysis unveiled a diminutive range, with particle sizes spanning between 1 and 50 nm, while the average diameter measured approximately 19.72 nm. Moreover, the morphological examination depicted a predominant spherical shape with some NPs being hexagonal, pyramidal and cylindrical in configuration (**Fig. 4.7.c; Fig. 4.7.d** & **Fig. 4.7.e**) [73]. Similarly, the FESEM analysis also confirmed that the NPs were of various shapes and sizes (**Fig. 4.7.f**) [74].

The CV analysis of the working electrode PEG/MA-AgNP/APTES/ITO was measured from -1.0 to 1.0 V at 100 mV/s in 0.2 M PBS buffer (pH = 6.5). During the

positive-going sweep of the CV, a few silver atoms on the surface of the NPs start to oxidize to form silver ions (Ag^+), resulting in a small increase in oxidation peak at around 0.1 V (**Fig. 4.7.g**) [75].

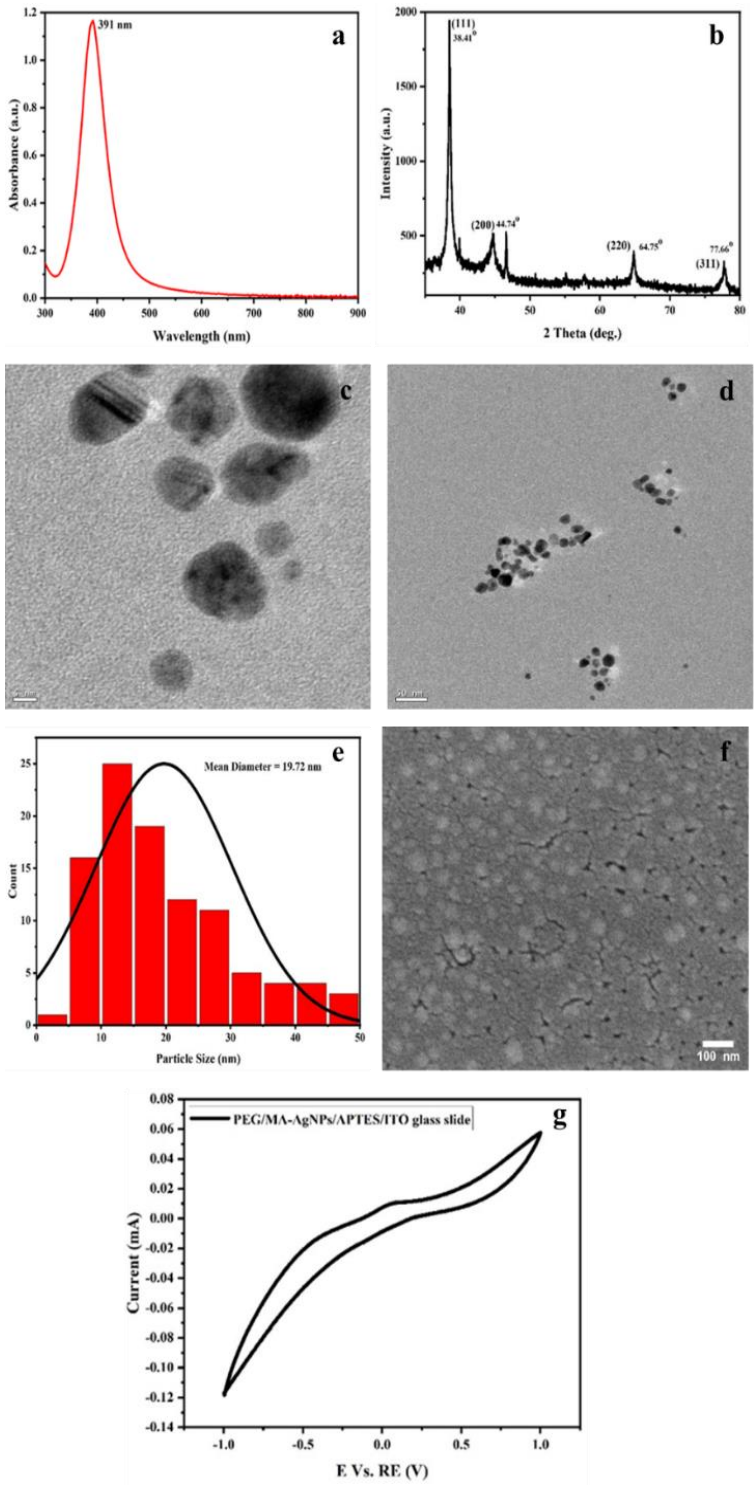

Figure 4.7: *Characterisation of PEG coated maleic acid functionalised AgNPs,* ***(a)*** *UV-Vis spectrum,* ***(b)*** *XRD pattern,* ***(c)*** *TEM images (high magnification),* ***(d)*** *TEM images (low magnification),* ***(e)*** *size distribution analysis from TEM,* ***(f)*** *FESEM image, and* ***(g)*** *cyclic voltametric analysis.*

4.5.3 Electrochemical sensing

4.5.3.1 Fabrication of the sensor

The ITO glass substrate (1 cm × 2 cm) was prepared by sequential cleaning as reported in the previous section 4.4.3.1.

The dry ITO glass was then immersed in a 1% APTES solution at 60°C for 1 h. After this, the substrate was thoroughly washed with DW to remove any unbound APTES from the surface. Next, 1 mL of PEG coated maleic acid functionalised AgNPs was drop-cast onto the APTES-treated ITO glass substrate, a process repeated four times to enhance deposition. The coated substrate was sintered at 60°C to ensure uniform NP coverage for 12 h (**Fig. 4.8**) [42,43].

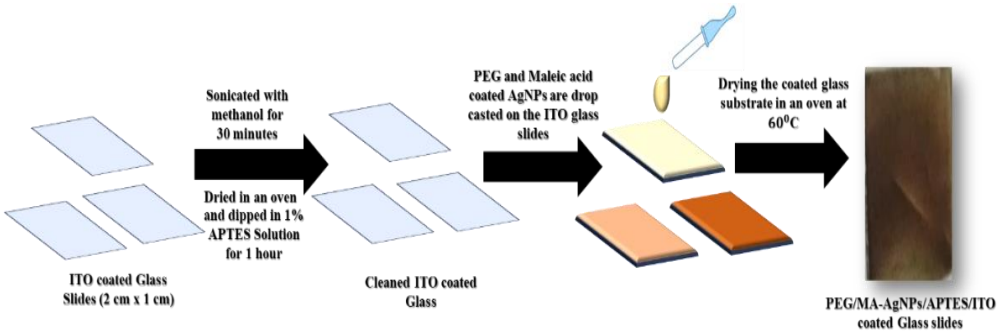

Figure 4.8: *Schematic illustration of fabrication of PEG/MA-AgNPs/APTES/ITO coated glass slides as the working electrode.*

4.5.3.2 Preliminary investigation of the working electrode

To verify the successful formation and electroactivity of the modified electrode, a ferricyanide test was conducted. Same protocol was implemented as outlined in the previous study (section 4.4.3.2.). Similar results were obtained in this case. [44].

4.5.3.3. Mechanism

In the electrochemical sensing of melamine on a PEG-capped/maleic acid-modified AgNPs coated ITO glass slide, both PEG and maleic acid play crucial roles in creating a highly sensitive and selective environment for detecting melamine.

Upon immersion of the electrode in the electrolyte containing melamine, the PEG-capped and maleic acid-functionalized AgNP-modified ITO electrode interacts with melamine molecules through a series of adsorption and electrochemical processes [76]. PEG, a stabilizing agent, prevents aggregation of AgNPs, ensuring a uniform NP distribution across the electrode surface. This stable distribution is critical for reliable electron transfer, providing an active, consistent surface area essential for electrochemical sensing [77]. The role of PEG extends beyond stabilization. Its hydrophilic nature creates a layer that improves the accessibility of melamine in aqueous solutions, allowing for efficient interaction between melamine molecules and the functionalized electrode, enhancing the sensor's selectivity toward melamine molecules.

Maleic acid, which is bound to the surface of AgNPs, introduces carboxyl (-COOH) functional groups that interact specifically with melamine's amine ($-NH_2$) groups. These interactions, mediated through hydrogen bonding and electrostatic attraction, facilitate the adsorption of melamine onto the electrode surface. Under slightly acidic conditions, melamine becomes protonated, and the negatively charged carboxyl groups of maleic acid may further attract melamine, reinforcing the selectivity and sensitivity of the sensor [78,79].

Once melamine is adsorbed onto the modified electrode, an applied potential during cyclic voltammetry induces the oxidation of melamine. The AgNPs play a pivotal role here by enhancing electron transfer, which amplifies the electrochemical response of melamine's oxidation. This oxidation is observed as an increased oxidation peak in the cyclic voltammogram, which is directly proportional to the melamine concentration. The PBS buffer surrounding the system provides a stable pH environment, ensuring consistent melamine oxidation and minimizing any interference from other ionic species in the solution [68].

The PEG and maleic acid synergistically enhance the electrode's performance by ensuring stability, facilitating melamine adsorption, and improving electron transfer efficiency. This leads to a marked increase in the oxidation peak, which serves as a quantitative indication of melamine presence in the sample. It turns out to be highly

selective and sensitive electrochemical sensor for melamine detection, utilizing PEG and maleic acid-modified AgNPs to achieve efficient and reproducible responses.

This oxidation peak, corresponding to the melamine concentration, provides a quantitative measure of melamine in the solution. Successive additions of melamine lead to systematic enhancement in the peak current, demonstrating the sensor's high sensitivity and rapid response. These lead to steady-state signals within seconds. In the cyclic voltametric response, no significant peaks appear in the potential window of -1.0 V to 1.0 V vs. Ag/AgCl in the absence of melamine. However, clear oxidation peaks emerge upon melamine addition.

The oxidation peak in CV for melamine detection on the PEG-capped/maleic acid-AgNP-modified ITO electrode is primarily due to the electrochemical oxidation of melamine adsorbed on the electrode surface.

The key chemical reactions can be represented as follows:

Initial adsorption on electrode surface: Melamine interacts with the functional groups on the modified AgNPs surface (maleic acid's carboxyl groups), resulting in stable adsorption.

Electrochemical oxidation of melamine: Upon applying an anodic potential, melamine undergoes electrochemical oxidation at the electrode surface. The oxidation process primarily involves its amine groups, which are susceptible to electron transfer under the applied potential.

Electron transfer to electrode: The released electrons flow through the electrode, resulting in the measurable oxidation current in the CV. The AgNPs on the ITO glass facilitates this electron transfer by providing conductive pathways, enhancing the current response due to their high surface area and conductivity.

4.5.3.4 Sensor performance metrics

The modified working electrode was further assessed for melamine detection using CV studies. For these measurements, the electrode setup included a PEG/MA-

AgNPs/APTES/ITO-coated glass slide as the working electrode, an Ag/AgCl electrode as the reference, and platinum as the counter electrode, with PBS and 0.1 M KCl (pH 6.5) as supporting electrolytes. The effective surface area of the working electrode was approximately 1 cm^2, and measurements were conducted over a potential range from -1.0 V to 1.0 V. In the absence of melamine, no significant peak was observed. However, upon adding melamine, a prominent oxidation peak appeared.

The oxidation peak current increased with higher concentrations of melamine in the milk supernatant, demonstrating a positive correlation between melamine concentration and current response. To evaluate the selectivity of the electrode, a bare electrode was used as a control (**Fig. 4.9**). The absence of any significant oxidation peak in this case confirmed the high selectivity of the PEG/MA-AgNPs/APTES/ITO-coated electrode for melamine detection. This is likely due to the catalytic effect of the MA-AgNPs towards melamine. This observation implies that the modified electrode's specific design enhances its sensitivity to melamine, while unmodified electrodes fail to generate detectable melamine signals [48,68].

The oxidation peak observed between 0.04 and 0.4 V in the presence of melamine is attributed to the melamine oxidation reaction facilitated by the PEG/MA-AgNPs on the electrode surface, as shown in **Fig. 4.10**. This distinct peak serves the basis for melamine detection, validating the electrode's activity and sensitivity. To quantify melamine, a calibration curve was generated by plotting the peak oxidation current against varying melamine concentrations, which exhibited a linear response with R^2 of 0.98. From this calibration curve, a LOD of 12.24 ppb was determined, while the sensitivity of the sensor was calculated to be 2.45×10^{-3} mA/ppb. This enhanced sensitivity, along with the straightforward and robust fabrication of the modified electrode, makes this sensor an effective tool for detecting trace amounts of melamine, even below permissible limits, as illustrated in **Fig. 4.11**. The recovery rate was found to be between 97.73%- 101.72%, which was calculated using equation 2.2 and error associated with the sensor was also calculated as reported in **Table 4.2**. [68].

The reproducibility of the sensor was evaluated by measuring peak current responses from multiple electrodes at the same melamine concentration. The consistent

peak currents across different electrodes demonstrated the sensor's reliability and reproducibility (**Fig. 4.12.a**). Reusability was assessed by conducting CV over several cycles on a single electrode, with stable CV responses confirming that the sensor could maintain performance across repeated uses (**Fig. 4.12.b**). To evaluate long-term stability, electrodes were stored in a vacuum to prevent oxidation and tested periodically over five days. The CV results showed minimal performance variations, indicating the electrodes remained functional for melamine detection after storage (**Fig. 4.12.c**). These findings highlight the sensor's durability and potential for practical use, supporting its commercialization as a reliable tool for melamine detection in diary safety and related applications [44,48,68].

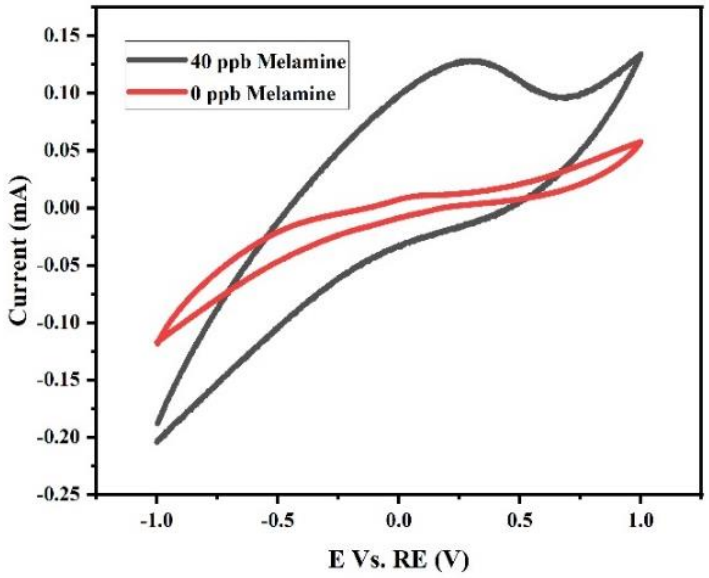

Figure 4.9: *Sensing performance of the PEG/MA-AgNPs/APTES ITO coated glass slides in absence and presence of melamine (Reference Electrode: Ag/AgCl; Auxiliary Electrode: Pt; Electrolyte: 0.2 M PBS and 0.4 M KCl at pH 6.5; Scan rate of 0.1 V/sec).*

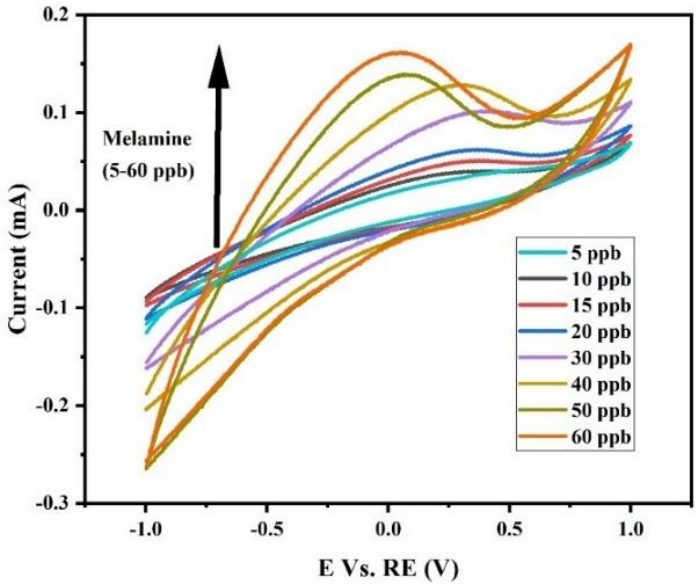

Figure 4.10: *CV Analysis of ITO electrode system fabricated with PEG/MA-AgNPs/APTES coated ITO glass slide in presence of different concentration of melamine in milk.* (*Reference Electrode: Ag/AgCl; Auxiliary Electrode: Pt; Electrolyte: 0.2 M PBS and 0.4 M KCl at pH 6.5; Scan rate of 0.1 V/sec).*

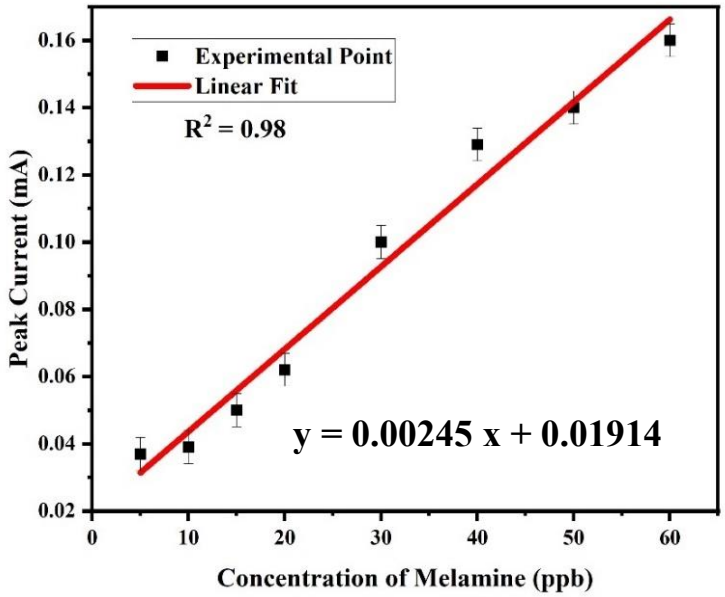

Figure 4.11: *Calibration graph between maximum oxidation current and the concentration of melamine in milk supernatant.*

Table 4.2: *Quantitative estimation of melamine in milk.*

SL. No.	Peak Current (mA)	Theoretical value of concentration (x_o) (ppb)	Experimental value of concentration (x) (ppb)	Error % $(\frac{x_0 - x}{x_0} \times 100)$
1	0.0792	25	24.51	1.96
2	0.1061	35	35.49	1.4
3	0.1269	45	43.98	2.26
4	0.1554	55	55.61	1.11
5	0.1612	57	57.98	1.72

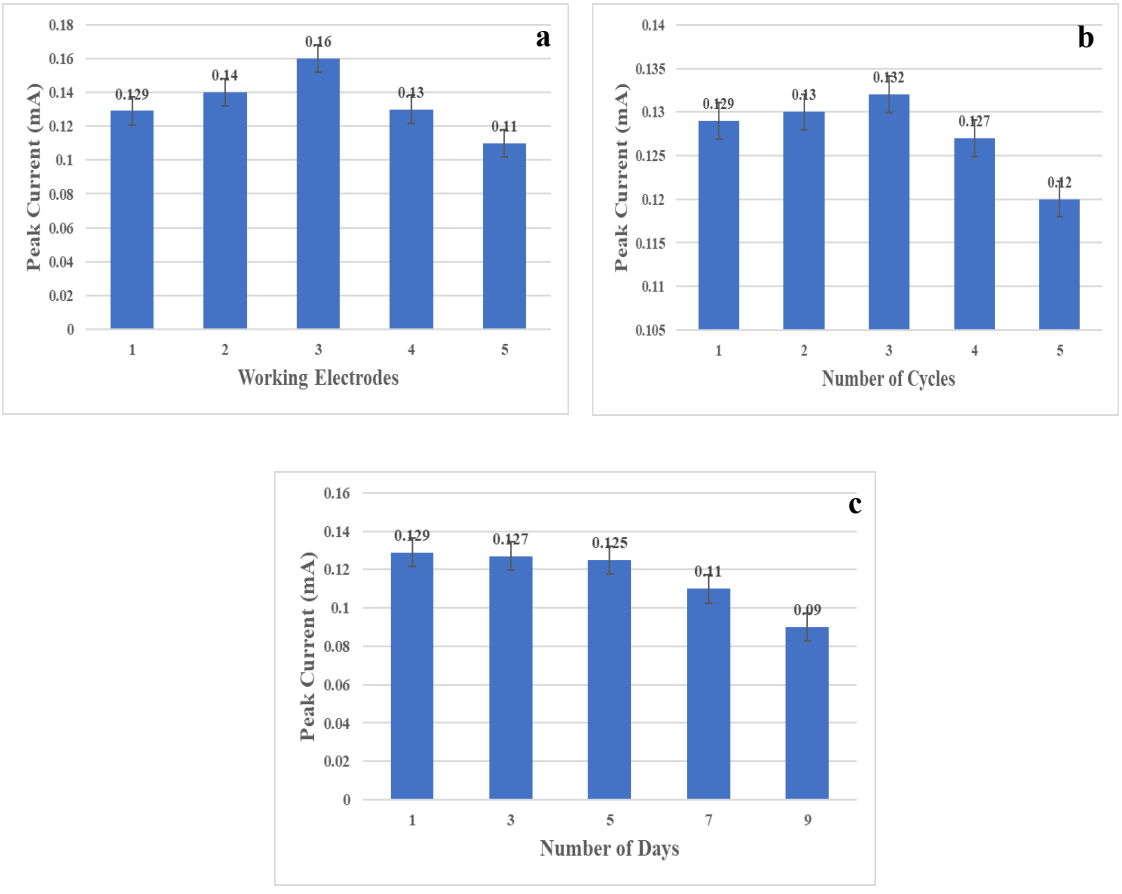

Figure 4.12: *CV response of the electrochemical sensor in the presence of melamine* ***(a)*** *with working electrode,* ***(b)*** *different cycles with the same electrode, and* ***(c)*** *with electrodes stored at different times (Electrolyte: 0.2 M PBS; Scan rate: 100 mV/s).*

4.6 Electrochemical sensing of hydrogen peroxide

Hydrogen peroxide is a versatile oxidizing agent widely used for its' mild antiseptic, bleaching, disinfecting, and preserving properties [80]. In dairy preservation, it is frequently utilised to extend the shelf life of milk by inhibiting microbial growth [81]. However, excessive or prolonged exposure to hydrogen peroxide through adulterated milk has been linked to various health issues. This underscores the importance of precise monitoring of its levels in milk to prevent associated health risks [82].

Standard analytical techniques for its detection include UV-Vis spectrophotometry, fluorimetry, chemiluminescence, and infrared spectrometry. The applicability of these methods is limited across complex sample types like milk, where sample composition can interfere with detection accuracy [83,84].

Electrochemical sensing has emerged as a highly efficient, rapid, and sensitive approach for its detection, particularly in complex matrices such as milk. By employing modified electrodes incorporating NMs, electrochemical sensors can detect hydrogen peroxide through oxidation-reduction reactions that yield an enhanced value of peak current directly proportional to its concentration. NMs play a critical role in this process, as their catalytic properties significantly enhance electron transfer rates, thus improving the sensitivity and selectivity of detection [85,86].

In electrochemical sensing of hydrogen peroxide in milk, cyclic voltammetry and amperometry are the most employed methods, as they provide precise, quantitative insights into its concentrations even at low levels [87]. CV, in particular, is advantageous due to its ability to detect redox reactions occurring at the electrode surface without additional reagents, enabling a simpler yet highly selective and sensitive approach [88].

Recent advancements have explored enzyme-immobilized electrodes and nanocomposite materials to further improve hydrogen peroxide detection capabilities, although challenges such as cost of fabrication, and stability of the working electrode still remain unexplored [89].

Some previous literatures have reported sensing of hydrogen peroxide in milk such as Ghosale *et al.,* in the year 2018 reported detection of hydrogen peroxide in hospital and beauty parlour wastewater by using AgNPs modified with PVA screen printed electrode (SPE). They obtained a linear calibration range between 1.0 mM to 0.5 mM, with a LOD value of 0.3 mM [89]. Another work by this group in the year 2016 reported detection of the same analyte by using paper electrode (PE) fabricated utilising AgNPs capped with octylamine which was also used for sensing of hydrogen peroxide in wastewater samples with a LOD of 0.5 μM [90]. Though these systems were designed for detection of hydrogen peroxide, but they could not detect the analyte in complicated complex matrix like milk with high accuracy and less LOD value.

To overcome this lacuna, this study introduces an electrochemical sensor that has been tailored for sensing of hydrogen peroxide in milk, addressing the demand for a reliable, affordable, and easily fabricated detection method. The sensor utilizes polyvinylpyrrolidone (PVP)-coated AgNPs, chosen for their exceptional conductivity, stability, and compatibility with complex biological matrices like milk. These properties make AgNPs an excellent choice for achieving highly sensitive electrochemical detection. The PVP coating not only stabilizes the AgNPs but also improves sensor performance by enhancing its interactions with hydrogen peroxide molecules, thereby increasing both sensitivity and selectivity for its detection in milk samples. This sensor design provides a robust, efficient, and practical solution for monitoring hydrogen peroxide levels in dairy products.

4.6.1 Synthesis of PVP functionalised AgNPs and pretreatment of milk

Synthesis of reducing and functionalising agent: 10 mM $AgNO_3$ solution was prepared by dissolving 0.169 g in 100 mL of DW. For uniform dissolution of the precursor salt the solution was stirred at room temperature for a duration of 10 min at a stirring rate of 600 rpm. Following which, the BRB extract was prepared, for which 50 g of BRB was chopped into small pieces, washed properly and dried in an oven at 100°C for 12 h. To this dried BRB, 200 mL of DW was added, and the resulting mixture was heated at 100°C for 1 ½ h. Then this extract was filtered twice by using Whatman filter paper no. 1. For functionalisation of NPs, 3% PVP solution was prepared for which 3 g of PVP was

dissolved in 100 mL of DW by stirring it at 60ºC for a duration of 3 h at a rate of 700 rpm. 0.1 M NaOH solution was prepared to adjust the pH of the solution [91,92].

Preparation of functionalised AgNPs: 40 mL of 10 mM $AgNO_3$ solution was stirred continuously to it 3.2 mL of BRB extract was added, and the solution was stirred at 700 rpm at 120ºC for a duration of 30 min. The colour of the solution slowly changed from pale yellow colour to deep brown colour indicating formation of NPs in the solution. Following this, the 5 mL of 3% PVP solution was added, and the resulting mixture was stirred at 800 rpm for 1 h at 60ºC. The pH of the solution was then adjusted to 7 by addition of 0.1 M NaOH. The resulting solution was brown in colour indicating formation of PVP functionalised AgNPs [91,92].

Pretreatment of milk: Same protocol was implemented as outlined in the previous study (section 2.A.1.1). After following this process, the resultant milk supernatant, was then spiked with various concentrations of hydrogen peroxide (10 to 500 ppb) for subsequent testing.

4.6.2 Characterisation of PVP functionalised AgNPs

Characterisation of the NPs were performed by following the previous protocol. UV–Vis analysis was performed where the NPs displayed an intense broad absorption peak at 441 nm (**Fig. 4.13.a**) [71].

Four distinct peaks were observed in the XRD pattern at 37.97°, 44.01°, 64.34°, and 77.34°, corresponding to the (111), (200), (220), and (311) planes, respectively. The presence of these characteristic diffraction peaks confirms that the synthesized AgNPs exhibit an FCC crystalline structure (**Fig. 4.13.b**) [72].

The size distribution analysis obtained from TEM study unveiled a diminutive range, with particle sizes spanning between 3 and 28 nm, while the average diameter measured approximately 11.97 nm. Moreover, the morphological examination depicted a predominantly spherical with some NPs hexagonal in configuration (**Fig. 4.13.c; Fig.**

4.13.d & **Fig. 4.13.e**). Similarly, for FESEM analysis was also performed which elucidated that the NPs were of spherical shapes (**Fig. 4.13.f**) [44,48].

A CV analysis was performed for the electrode PVP/AgNP/APTES/ITO between -1.5 to 1.5 V at 100 mV/s., with 0.2 M phosphate buffer (pH = 7.2) as the electrolyte. At a certain potential, a few silver atoms on the surface of the NPs start to oxidize to form silver ions (Ag^+), resulting in a small increase in oxidation peak at around 1.0 V (**Fig. 4.13.g**) [68,89,90].

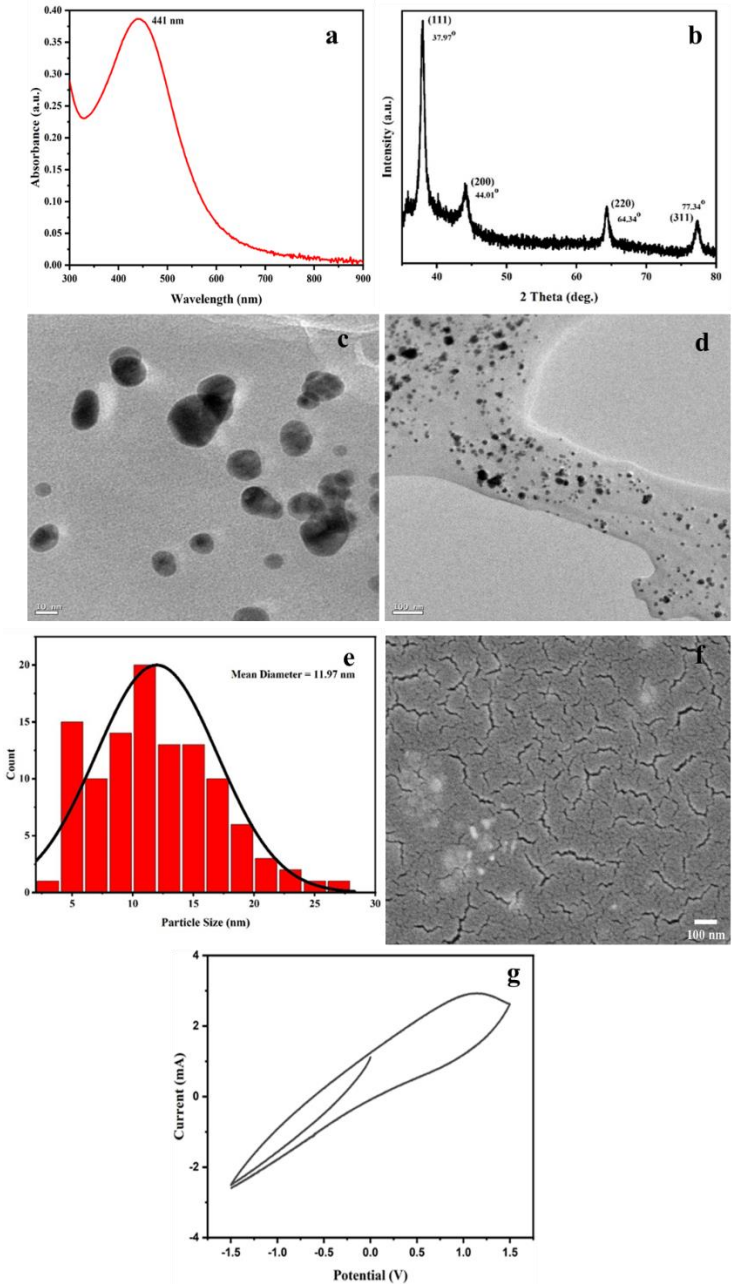

Figure 4.13: *Characterisation of PVP coated AgNPs,* ***(a)*** *UV-Vis spectrum,* ***(b)*** *XRD pattern,* ***(c)*** *TEM images (high magnification),* ***(d)*** *TEM images (low magnification),* ***(e)*** *size distribution analysis from TEM,* ***(f)*** *FESEM image, and* ***(g)*** *cyclic voltametric analysis.*

4.6.3 Electrochemical sensing

4.6.3.1 Fabrication of the Sensor

The ITO glass substrate (1 cm × 2 cm) was prepared by sequential cleaning as reported (section 4.5.3.1).

The dry ITO glass was then immersed in a 1% APTES solution at 60°C for 1 hour. After this, the substrate was thoroughly washed with DW to remove any unbound APTES from the surface. Next, 1 mL of PVP functionalised AgNPs was drop-cast onto the APTES-treated ITO glass substrate, a process being repeated four times to enhance deposition. The coated substrate was sintered at 60°C to ensure uniform NPs coverage for 8 h (**Fig. 4.14**) [42,43].

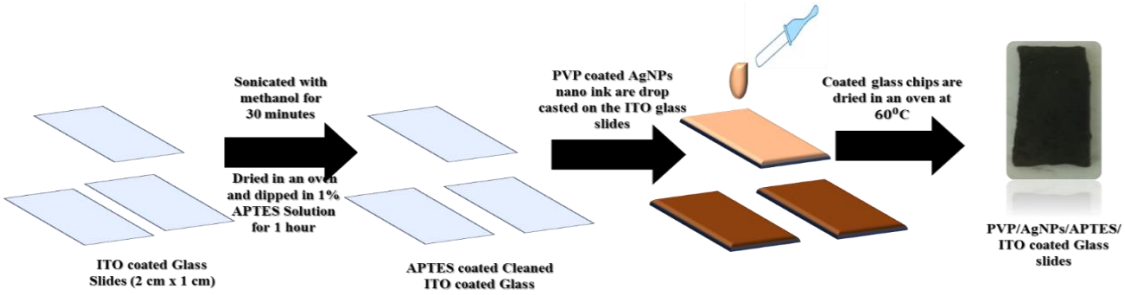

Figure 4.14: *Schematic Illustration of fabrication of PVP/AgNPs/APTES/ITO coated glass slides as the working electrode.*

4.6.3.2 Preliminary investigation of the working electrode

To verify the successful formation and electroactivity of the modified electrode, a ferricyanide test was conducted. Same protocol was implemented as outlined in the previous study (section 4.4.3.2) Similar results were observed in this case [44].

4.6.3.3 Mechanism

The electrochemical sensing mechanism for hydrogen peroxide using PVP-coated AgNPs-modified ITO electrode relies on the catalytic activity of the AgNPs to facilitate electron transfer between hydrogen peroxide and the electrode surface. When hydrogen peroxide was introduced to the sensor, it undergoes a reduction reaction at the AgNPs-modified

electrode, where the PVP coating on AgNPs helps to stabilize the NPs and enhance their dispersion, ensuring consistent catalytic sites across the electrode surface. The AgNPs act as electron mediators, accelerating the redox reaction of hydrogen peroxide at the electrode surface and generating a measurable current. Specifically, hydrogen peroxide was reduced at the electrode surface, where it accepted electrons from the electrode, resulting in a reduction peak in the cyclic voltammetry measurement [89,90].

As the concentration of hydrogen peroxide increases, the number of hydrogen peroxide molecules available at the electrode surface for reduction also rises. This leads to a higher electron transfer rate as more hydrogen peroxide molecules participate in the redox reaction, producing a greater current and a more pronounced reduction peak in the CV graph. The observed increase in reduction peak intensity with higher hydrogen peroxide concentrations is therefore directly related to the higher electron exchange rate facilitated by the AgNPs-modified electrode. The linear relationship between the concentration of H_2O_2 and the reduction current allows for the precise quantification of hydrogen peroxide levels, making this sensor design an effective approach for monitoring hydrogen peroxide concentrations in complex matrices like milk [89]. Here, AgNPs act as catalytic centres for electron transfer, while PVP stabilizes the nanoparticles and ensures good dispersion and accessibility, leading to a highly sensitive and stable sensor.

This reaction mechanism highlights the role of AgNPs in providing a high surface area and efficient electron mediation, facilitating the reduction of hydrogen peroxide and enabling accurate and sensitive electrochemical detection.

The electrochemical reduction of hydrogen peroxide at the PVP-AgNPs modified ITO electrode occurs through the following steps:

Adsorption of hydrogen peroxide: Hydrogen peroxide molecules diffuse from the bulk solution and adsorb onto the surface of the PVP-coated AgNPs, which are dispersed uniformly across the ITO electrode surface.

Electron transfer: The AgNPs, with their excellent catalytic properties, facilitate the transfer of electrons from the electrode surface to the hydrogen peroxide molecules. PVP coating stabilizes the AgNPs, ensuring effective interactions with hydrogen peroxide.

Reduction Reaction of Hydrogen peroxide: At the electrode surface, the adsorbed H_2O_2 undergoes an electrochemical reduction reaction in slightly acidic medium [89,90] (reaction 4.3):

$$Ag^0\text{-}\ H_2O_2 + 2H^+ + 2e^- \rightarrow 2H_2O + Ag^+ \qquad (\mathbf{4.3})$$

Here, each hydrogen peroxide molecule accepts two electrons, reducing to water.

Generation of Reduction Current: The reduction of hydrogen peroxide results in a flow of electrons to the electrode, generating a measurable reduction current. This current is directly proportional to its concentration of in milk [90].

4.6.3.4 Sensor performance metrics

The modified working electrode was further assessed for hydrogen peroxide detection using CV studies. For these measurements, the electrode setup included a PVP/AgNPs/APTES/ITO-coated glass slide as the working electrode, an Ag/AgCl electrode as the reference, and platinum as the counter electrode, with 0.2 M PBS and 0.4 M KCl (pH 5.2) as supporting electrolyte. The effective surface area of the working electrode was approximately 1 cm^2, and measurements were conducted over a potential range from -1.0 V to 1.0 V. In the absence of hydrogen peroxide, no significant peak was observed. However, upon adding hydrogen peroxide, a prominent reduction peak appeared.

The reduction peak current increased with higher concentrations of hydrogen peroxide in the milk supernatant, demonstrating a positive correlation between hydrogen peroxide concentration and current response (**Fig. 4.15**). The absence of any significant oxidation peak in this case confirmed the high selectivity of the PVP/AgNPs/APTES/ITO-coated electrode for hydrogen peroxide detection, likely due to the catalytic effect of the AgNPs which formed complex with hydrogen peroxide. This observation implies that the modified electrode's specific design enhances its sensitivity to hydrogen peroxide, while unmodified electrodes fail to generate detectable hydrogen peroxide signals.

The reduction peak observed between -0.6 and -0.3 V in the presence of hydrogen peroxide is attributed to the hydrogen peroxide reduction reaction facilitated by the PVP/AgNPs on the electrode surface, as shown in **Fig. 4.16**. In the first step, PVP-Ag^0 interacts with H_2O_2 to form a complex, PVP-Ag^{0}-H_2O_2. In the next step, the complex is electrochemically reduced to give PVP-Ag^+ and H_2O which can be seen as a reduction peak. This makes the catalytic cycle. Therefore, a high catalytic current was observed on PVP/AgNPs/APTES electrode. This distinct peak serves as a measurable signal for hydrogen peroxide detection, validating the electrode's activity and sensitivity. To quantify hydrogen peroxide, a calibration curve was plotted between the peak oxidation current against varying hydrogen peroxide concentrations, which exhibited a linear response with R^2 of 0.97. From this calibration curve, a LOD of 5.19 ppb was determined, while the sensitivity of the sensor was calculated to be 6.35×10^{-3} mA/ppb. This enhanced sensitivity, along with the straightforward and robust fabrication of the modified electrode, makes this sensor an effective tool for detecting trace amounts of hydrogen peroxide, even below permissible limits, as illustrated in **Fig. 4.17**. The recovery rate was found to be between 98.73%- 100.45%, which was calculated using equation 2.2 and error associated with the sensor was also calculated as reported in **Table 4.3**. [89-92].

The sensor's reproducibility was assessed by recording peak current response across multiple electrodes, each tested at the same hydrogen peroxide concentration. This demonstrated consistent peak currents across different electrodes, confirming the sensor's reliability and reproducibility (**Fig. 4.18.a**). Additionally, the reusability of the sensor was evaluated by performing CV over multiple cycles on a single electrode, where the consistent CV responses across these cycles indicated that the sensor maintained stable performance and could be reused effectively (**Fig. 4.18.b**). To further assess the sensor's stability over time, electrodes were stored in vacuum to prevent oxidation and were periodically tested over a five-day span. CV measurements taken at intervals revealed only minor variations in performance, indicating that the electrodes retained functionality for hydrogen peroxide detection even after extended stability over time (**Fig. 4.18.c**).

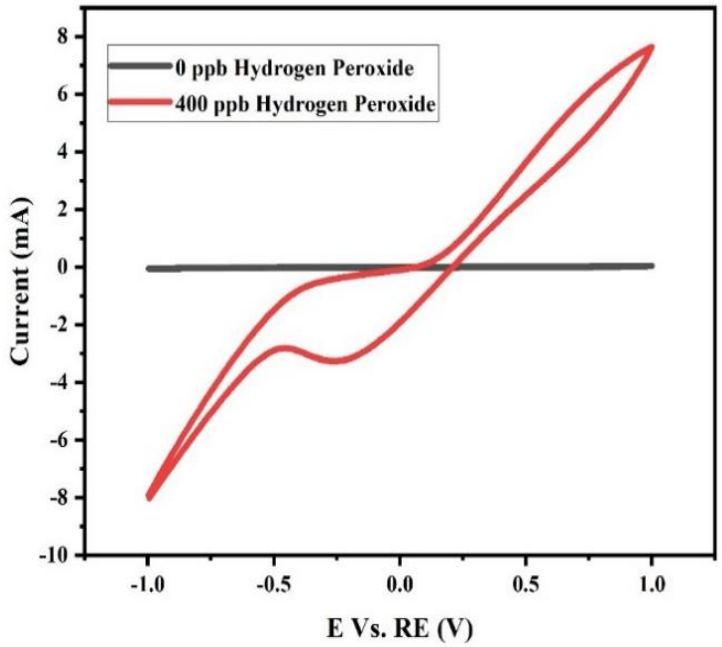

Figure 4.15: *Sensing performance of the PVP/AgNPs/APTES ITO coated glass slides in absence and presence of hydrogen peroxide (Reference Electrode: Ag/AgCl; Auxiliary Electrode: Pt; Electrolyte: 0.2 M PBS and 0.4 M KCl at pH 5.2; Scan rate of 0.1 V/sec).*

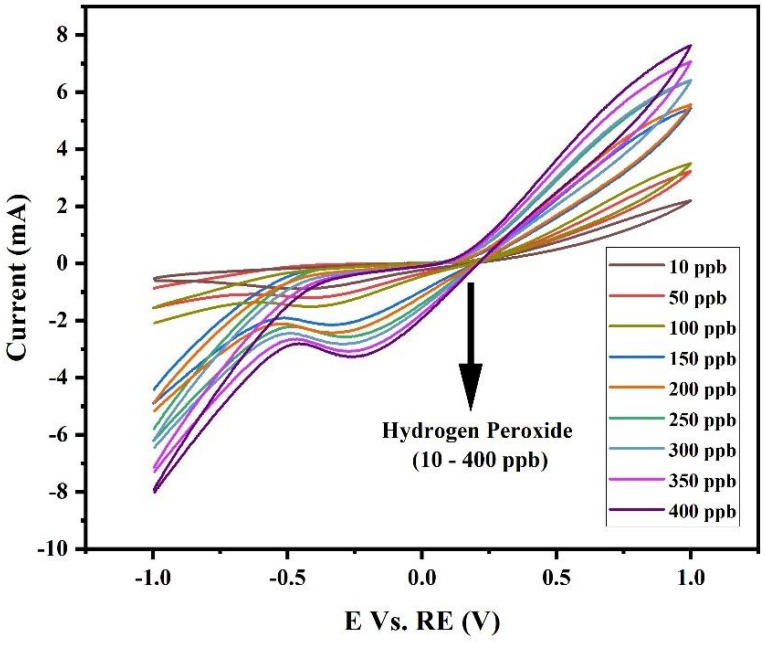

Figure 4.16: *CV Analysis of ITO electrode system fabricated with PVP/AgNPs/APTES coated ITO glass slide in presence of different concentration of hydrogen peroxide in milk (Reference Electrode: Ag/AgCl; Auxiliary Electrode: Pt; Electrolyte: 0.2 M PBS and 0.4 M KCl at pH 5.2; Scan rate of 0.1 V/sec).*

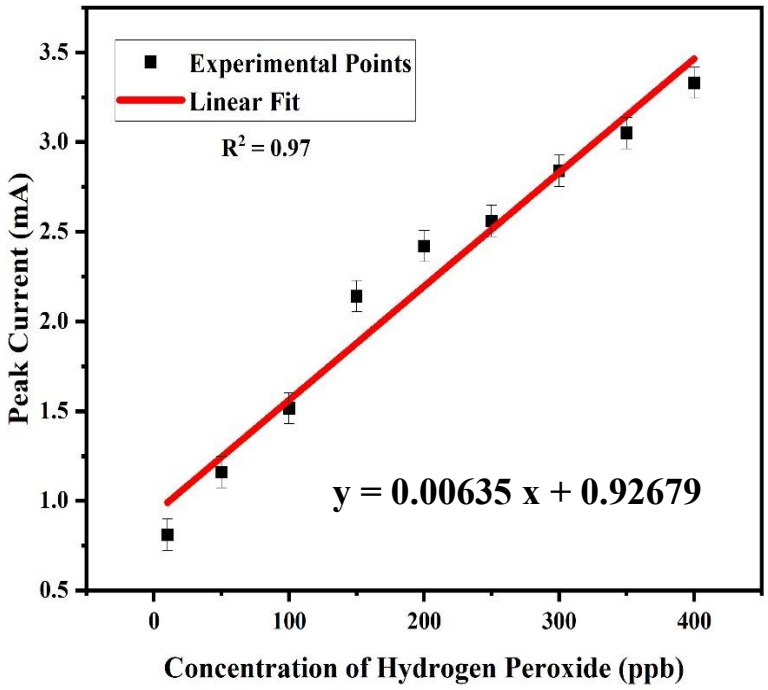

Figure 4.17: *Calibration graph plotted between maximum reduction current (negative peak current) vs. the concentration of hydrogen peroxide in milk supernatant.*

Table 4.3: *Quantitative estimation of hydrogen peroxide in milk.*

SL. No.	Negative peak current (mA)	Theoretical value of concentration (x_o) (ppb)	Experimental value of concentration (x) (ppb)	Error % $(\frac{x_0 - x}{x_0} \times 100)$
1	1.397	75	74.05	1.26
2	1.717	125	124.44	0.45
3	2.041	175	175.46	0.26
4	2.362	225	226.02	0.45
5	2.679	275	275.94	0.34

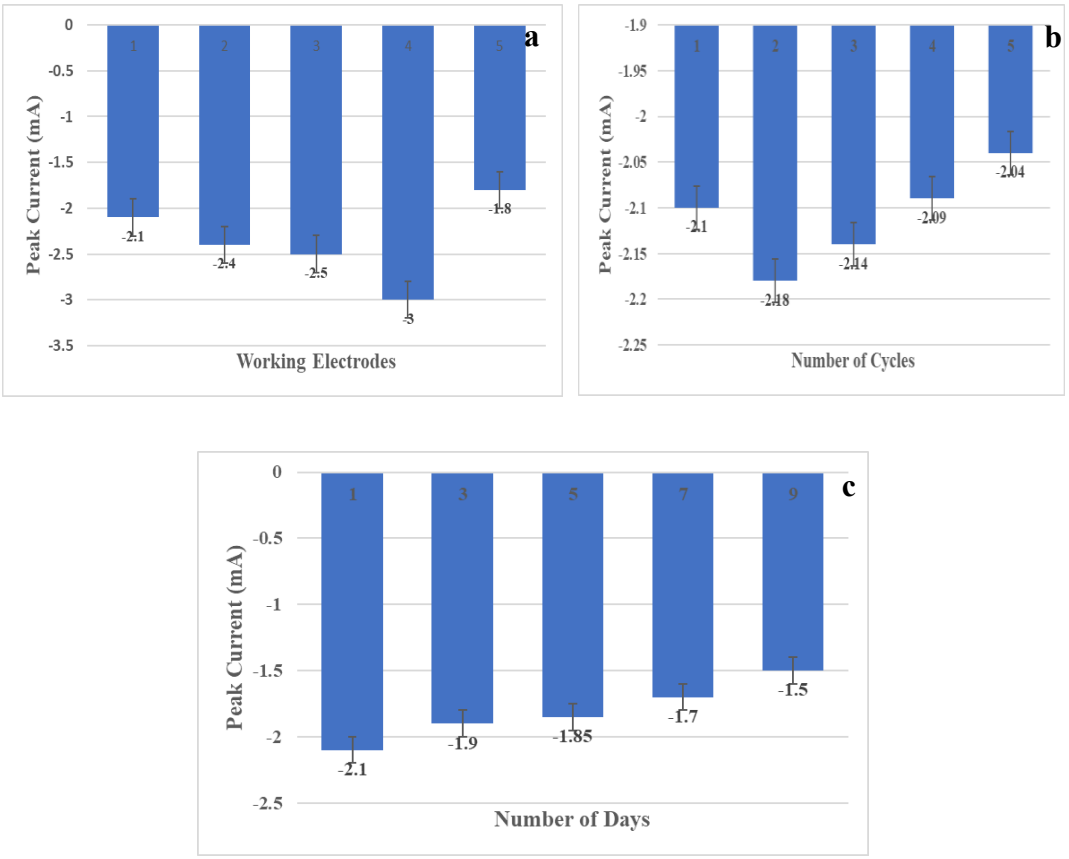

Figure 4.18: *CV response of the working electrodes in the presence of hydrogen peroxide* ***(a)*** *with different set of electrodes,* ***(b)*** *different cycles with the same electrode, and* ***(c)*** *with electrode stored at different times (Electrolyte: 0.2 M PBS; Scan rate: 100 mV/s).*

4.7 Conclusion

This chapter highlights the successful development and application of three distinct NP-modified electrode platforms for the sensitive, selective, and cost-effective detection of adulterants in milk, including urea, melamine, and hydrogen peroxide. The green tea-reduced APTES coated AuNPs-modified electrode demonstrated non-enzymatic urea detection with high selectivity and sensitivity, achieving a detection limit of 4.02 ppm and a recovery rate between 95.05%-99.44%, supported by stable and reproducible electrochemical responses. The PEG/maleic acid-coated AgNPs electrode enabled precise melamine quantification with a detection limit of 12.24 ppb, a recovery rate between 97.73%-101.72% accompanied by exceptional reproducibility and stability. Additionally, the PVP-coated AgNP-modified electrode facilitated hydrogen peroxide detection with a detection limit of 5.19 ppb, a recovery rate between 98.73%-100.45%, and enhanced sensitivity through catalytic electron transfer.

All three sensors demonstrated robust electrochemical performance, excellent reproducibility, and stability under various conditions, supporting their potential for long-term storage and repeated use. Compared to conventional detection methods requiring expensive and complex instruments, these platforms provide portable, cost-effective alternatives suitable for rapid, on-site analysis. Their scalability, reliability, and user-friendly design position them as promising candidates for commercialization, offering practical solutions for real-time monitoring of milk adulterants.

References

[1] Wang, D., Pillai, S. C., Ho, S. H., Zeng, J., Li, Y., and Dionysiou, D. D. Plasmonic-based nanomaterials for environmental remediation. *Applied Catalysis B: Environmental*, 237: 721-741, 2018.

[2] Dahlin, A. B., Dielacher, B., Rajendran, P., Sugihara, K., Sannomiya, T., Zenobi-Wong, M., and Vörös, J. Electrochemical plasmonic sensors. *Analytical and Bioanalytical Chemistry*, 402: 1773-1784, 2012.

[3] Chen, A., and Chatterjee, S. Nanomaterials based electrochemical sensors for biomedical applications. *Chemical Society Reviews*, 42(12): 5425-5438, 2013.

[4] Nemčeková, K., and Labuda, J. Advanced materials-integrated electrochemical sensors as promising medical diagnostics tools: A review. *Materials Science and Engineering: C*, 120: 111751, 2021.

[5] Bilger, D., Homayounfar, S. Z., and Andrew, T. L. A critical review of reactive vapor deposition for conjugated polymer synthesis. *Journal of Materials Chemistry C*, 7(24): 7159-7174, 2019.

[6] Cheng, X. R., Wallace, G. Q., Lagugné-Labarthet, F., and Kerman, K. Au nanostructured surfaces for electrochemical and localized surface plasmon resonance-based monitoring of α-synuclein–small molecule interactions. *ACS Applied Materials & Interfaces*, 7(7): 4081-4088, 2015.

[7] Fang, Y., Wang, H., Yu, H., Liu, X., Wang, W., Chen, H. Y., and Tao, N. J. Plasmonic imaging of electrochemical reactions of single nanoparticles. *Accounts of chemical research*, 49(11): 2614-2624, 2016.

[8] Dahlin, A. B., Dielacher, B., Rajendran, P., Sugihara, K., Sannomiya, T., Zenobi-Wong, M., and Vörös, J. Electrochemical plasmonic sensors. *Analytical and Bioanalytical Chemistry*, 402: 1773-1784, 2012.

[9] Poonia, A., Jha, A., Sharma, R., Singh, H. B., Rai, A. K., and Sharma, N. Detection of adulteration in milk: A review. *International journal of dairy technology*, 70(1): 23-42, 2017.

[10] Lu, S. M., Peng, Y. Y., Ying, Y. L., and Long, Y. T. Electrochemical sensing at a confined space. *Analytical chemistry*, 92(8): 5621-5644, 2020.

[11] Sakthivel, K., Balasubramanian, S., Chang-Chien, G. P., Wang, S. F., Ahammad, F. N. U., Billey, W., and Sekhar, P. Advances in Electrochemical Sensors: Improving Food Safety, Quality, and Traceability. *ECS Sensors Plus*, 2024.

[12] Ghaani, M., Azimzadeh, M., Büyüktaş, D., Carullo, D., and Farris, S. Electrochemical Sensors in the Food Sector: A Review. *Journal of Agricultural and Food Chemistry*, 2024.

[13] Lambrini, K., Aikaterini, F., Konstantinos, K., Christos, I., Ioanna, P. V., and Areti, T. Milk nutritional composition and its role in human health. *Journal of Pharmacy and Pharmacology*, 9: 8-13, 2021.

[14] Azad, T., and Ahmed, S. Common milk adulteration and their detection techniques. *International Journal of Food Contamination*, 3: 1-9, 2016.

[15] Kailasapathy, K. Chemical composition, physical, and functional properties of milk and milk ingredients. *Dairy processing and quality assurance*, 77-105, 2015.

[16] Popescu, A., and Angel, E. Cow raw milk quality and its factors of influence in relationship with milk price. *Scientific Papers Series Management, Economic Engineering in Agriculture & Rural Development*, 19(1), 2019.

[17] Ionescu, A. D., Cîrîc, A. I., and Begea, M. A review of milk frauds and adulterations from a technological perspective. *Applied Sciences*, 13(17): 9821, 2023.

[18] Hof, G., Vervoorn, M. D., Lenaers, P. J., and Tamminga, S. Milk urea nitrogen as a tool to monitor the protein nutrition of dairy cows. *Journal of dairy science*, 80(12): 3333-3340, 1997.

[19] Banti, M. Food adulteration and some methods of detection, review. *International Journal of Nutrition and Food Sciences*, 9(3): 86-94, 2020.

[20] Vanholder, R., Gryp, T., and Glorieux, G. Urea and chronic kidney disease: the comeback of the century? (in uraemia research). *Nephrology Dialysis Transplantation*, 33(1): 4-12, 2018.

[21] Singh, P., and Gandhi, N. Milk preservatives and adulterants: processing, regulatory and safety issues. *Food Reviews International*, 31(3): 236-261, 2015.

[22] Mashhadban, K. F., Gorgani, L., and Darzi, G. N. Enzymatic Electrochemical Biosensors for Urea Detection: A Review. *Sensors and Actuators A: Physical*, 115499, 2024.

[23] Singh, M., Verma, N., Garg, A. K., and Redhu, N. Urea biosensors. *Sensors and actuators B: chemical*, 134(1): 345-351, 2008.

[24] Botewad, S. N., Gaikwad, D. K., Girhe, N. B., Thorat, H. N., and Pawar, P. P. Urea biosensors: A comprehensive review. *Biotechnology and Applied Biochemistry*, 70(2): 485-501, 2023.

[25] Francis, P. S., Lewis, S. W., and Lim, K. F. Analytical methodology for the determination of urea: current practice and future trends. *TrAC trends in analytical chemistry*, 21(5): 389-400, 2002.

[26] Singh, S., Sharma, M., and Singh, G. Recent advancements in urea biosensors for biomedical applications. *IET nanobiotechnology*, 15(4): 358-379, 2021.

[27] Chou, J. C., Wu, C. Y., Kuo, P. Y., Lai, C. H., Nien, Y. H., Wu, Y. X., Xiang, Y., Lin, S.H. and Liao, Y. H. The flexible urea biosensor using magnetic nanoparticles. *IEEE Transactions on Nanotechnology*, 18: 484-490, 2019.

[28] Srivastava, R. K., Srivastava, S., Narayanan, T. N., Mahlotra, B. D., Vajtai, R., Ajayan, P. M., and Srivastava, A. Functionalized multilayered graphene platform for urea sensor. *ACS nano*, 6(1): 168-175, 2012.

[29] Deng, H. H., Hong, G. L., Lin, F. L., Liu, A. L., Xia, X. H., and Chen, W. Colorimetric detection of urea, urease, and urease inhibitor based on the peroxidase-like activity of gold nanoparticles. *Analytica chimica acta*, 915: 74-80, 2016.

[30] Mashhadban, K. F., Gorgani, L., and Darzi, G. N. Enzymatic Electrochemical Biosensors for Urea Detection: A Review. *Sensors and Actuators A: Physical*, 115499, 2024.

[31] Quadrini, L., Laschi, S., Ciccone, C., Catelani, F., and Palchetti, I. Electrochemical methods for the determination of urea: Current trends and future perspective. *TrAC Trends in Analytical Chemistry*, 117345, 2023.

[32] Ho, W. O., Krause, S., McNeil, C. J., Pritchard, J. A., Armstrong, R. D., Athey, D., and Rawson, K. Electrochemical sensor for measurement of urea and creatinine in serum based on ac impedance measurement of enzyme-catalyzed polymer transformation. *Analytical Chemistry*, 71(10): 1940-1946, 1999.

[33] Magar, H. S., Hassan, R. Y., and Abbas, M. N. Non-enzymatic disposable electrochemical sensors based on CuO/Co3O4@ MWCNTs nanocomposite modified screen-printed electrode for the direct determination of urea. *Scientific Reports*, 13(1): 2034, 2023.

[34] Liu, J., Siavash Moakhar, R., Sudalaiyadum Perumal, A., Roman, H. N., Mahshid, S., and Wachsmann-Hogiu, S. An AgNP-deposited commercial electrochemistry test strip as a platform for urea detection. *Scientific reports*, 10(1): 9527, 2020.

[35] Sharma, P., and Sharma, B. Phytofabricated silver nanoparticle-modified glass electrodes for non-enzymatic potentiometric urea sensing. *AIP Conference Proceedings,* 3149(1), 2024.

[36] Lee, Y. J., Ahn, E. Y., and Park, Y. Shape-dependent cytotoxicity and cellular uptake of gold nanoparticles synthesized using green tea extract. *Nanoscale research letters*, 14(1): 129, 2019.

[37] Amendola, V., and Meneghetti, M. Size evaluation of gold nanoparticles by UV− vis spectroscopy. *The Journal of Physical Chemistry C*, 113(11): 4277-4285, 2009.

[38] Sathiyaraj, S., Suriyakala, G., Gandhi, A. D., Babujanarthanam, R., Almaary, K. S., Chen, T. W., and Kaviyarasu, K. Biosynthesis, characterization, and antibacterial activity of gold nanoparticles. *Journal of Infection and Public Health*, 14(12): 1842-1847, 2021.

[39] Boruah, S. K., Boruah, P. K., Sarma, P., Medhi, C., and Medhi, O. K. Green synthesis of gold nanoparticles using Camellia sinensis and kinetics of the reaction. *Advance Material Letters*, 3(6): 481-6, 2012.

[40] Raghunandan, D., Bedre, M. D., Basavaraja, S., Sawle, B., Manjunath, S. Y., and Venkataraman, A. Rapid biosynthesis of irregular shaped gold nanoparticles from macerated aqueous extracellular dried clove buds (Syzygium aromaticum) solution. *Colloids and Surfaces B: Biointerfaces*, 79(1): 235-240, 2010.

[41] Zakaria, N. D., Omar, M. H., Ahmad Kamal, N. N., Abdul Razak, K., Sönmez, T., Balakrishnan, V., and Hamzah, H. H. Effect of supporting background electrolytes on the nanostructure morphologies and electrochemical behaviors of electrodeposited gold nanoparticles on glassy carbon electrode surfaces. *ACS omega*, 6(38): 24419-24431, 2021.

[42] Wang, L., Mao, W., Ni, D., Di, J., Wu, Y., and Tu, Y. Direct electrodeposition of gold nanoparticles onto indium/tin oxide film coated glass and its application for electrochemical biosensor. *Electrochemistry Communications*, 10(4): 673-676, 2008.

[43] Nor, N. M., Lockman, Z., and Razak, K. A. Study of ITO glass electrode modified with iron oxide nanoparticles and nafion for glucose biosensor application. *Procedia Chemistry*, 19: 50-56, 2016.

[44] Liu, J., Siavash Moakhar, R., Sudalaiyadum Perumal, A., Roman, H. N., Mahshid, S., and Wachsmann-Hogiu, S. An AgNP-deposited commercial electrochemistry test strip as a platform for urea detection. Scientific reports, 10(1): 9527, 2020.

[45] Aydın, E. B., and Sezgintürk, M. K. Indium tin oxide (ITO): A promising material in biosensing technology. *TrAC Trends in Analytical Chemistry*, 97: 309-315, 2017.

[46] Wang, J., Wang, L., Di, J., and Tu, Y. Electrodeposition of gold nanoparticles on indium/tin oxide electrode for fabrication of a disposable hydrogen peroxide biosensor. *Talanta*, 77(4): 1454-1459, 2009.

[47] Lian, H. T., Liu, B., Chen, Y. P., and Sun, X. Y. A urea electrochemical sensor based on molecularly imprinted chitosan film doping with CdS quantum dots. *Analytical biochemistry*, 426(1): 40-46, 2012.

[48] Korkut, S., Uzuncar, S., Kilic, M. S., and Hazer, B. Electrochemical determination of urea using a gold nanoparticle-copolymer coated-enzyme modified gold electrode. *Instrumentation Science & Technology*, 47(1): 1-18, 2019.

[49] Vedharathinam, V., and Botte, G. G. Understanding the electro-catalytic oxidation mechanism of urea on nickel electrodes in alkaline medium. *Electrochimica Acta*, 81: 292-300, 2012.

[50] Elgrishi, N., Rountree, K. J., McCarthy, B. D., Rountree, E. S., Eisenhart, T. T., and Dempsey, J. L. A practical beginner's guide to cyclic voltammetry. *Journal of chemical education*, 95(2): 197-206, 2018.

[51] Zoski, C. G., Leddy, J., Bard, A. J., Faulkner, L. R., and White, H. S. Electrochemical Methods: Fundamentals and Applications, 3e Student Solutions Manual. *John Wiley & Sons*, 2024.

[52] Alwael, H., Alharthi, A. S., Dabi, M. M., Oubaha, M., and El-Shahawi, M. S. A highly sensitive electrochemical sensing probe incorporating classical Berthelot's reaction and glassy carbon electrode for measuring ultra-trace levels of ammonia/NH4+ in water. *Electrochemistry Communications*, 162: 107686, 2024.

[53] Dorieh, A., Pour, M. F., Movahed, S. G., Pizzi, A., Selakjani, P. P., Kiamahalleh, M. V., ... and Aghaei, R. A review of recent progress in melamine-formaldehyde resin-based nanocomposites as coating materials. *Progress in Organic Coatings*, 165: 106768, 2022.

[54] Handford, C. E., Campbell, K., and Elliott, C. T. Impacts of milk fraud on food safety and nutrition with special emphasis on developing countries. *Comprehensive Reviews in Food Science and Food Safety*, 15(1): 130-142, 2016.

[55] Chang, H., Shi, X., Shen, W., Wang, W., and Yue, Z. Characterization of melamine-associated urinary stones in children with consumption of melamine-contaminated infant formula. *Clinica Chimica Acta*, 413(11-12): 985-991, 2012.

[56] Li, Q., Song, P., and Wen, J. Melamine and food safety: a 10-year review. *Current Opinion in Food Science*, 30: 79-84, 2019.

[57] Sun, F., Ma, W., Xu, L., Zhu, Y., Liu, L., Peng, C., Wang, L., Kuang, H.., and Xu, C. Analytical methods and recent developments in the detection of melamine. *TrAC Trends in Analytical Chemistry*, 29(11): 1239-1249, 2010.

[58] Ritota, M., and Manzi, P. Melamine detection in milk and dairy products: traditional analytical methods and recent developments. *Food analytical methods*, 11: 128-147, 2018.

[59] Lin, M. A review of traditional and novel detection techniques for melamine and its analogues in foods and animal feed. *Frontiers of Chemical Engineering in China*, 3: 427-435, 2009.

[60] Yu, H., Tao, Y., Chen, D., Wang, Y., Liu, Z., Pan, Y., Huang, L., Peng, D., Dai, M., Liu, Z., and Yuan, Z. Development of a high-performance liquid chromatography method and a liquid chromatography–tandem mass spectrometry method with pressurized liquid extraction for simultaneous quantification and confirmation of cyromazine, melamine and its metabolites in foods of animal origin. *Analytica chimica acta*, 682(1-2): 48-58, 2010.

[61] Kalambate, R. P., Kalambate, P. K., and Laiwattanapaisal, W. Revolutionizing melamine detection: Cutting-edge advances from traditional analyses to state-of-the-art electrochemical sensors. *Next Materials*, 3: 100085, 2024.

[62] Kaur, G., Kaur, A., and Kaur, H. Review on nanomaterials/conducting polymer-based nanocomposites for the development of biosensors and electrochemical sensors. *Polymer-Plastics Technology and Materials*, 60(5): 504-521, 2021.

[63] Kant, T., Shrivas, K., Dewangan, K., Kumar, A., Jaiswal, N. K., Deb, M. K., and Pervez, S. Design and development of conductive nanomaterials for electrochemical sensors: a modern approach. Materials Today Chemistry, 24: 100769, 2022.

[64] El Rhazi, M., Majid, S., Elbasri, M., Salih, F. E., Oularbi, L., and Lafdi, K. Recent progress in nanocomposites based on conducting polymer: application as electrochemical sensors. *International Nano Letters*, 8: 79-99, 2018.

[65] Daizy, M., Tarafder, C., Al-Mamun, M. R., Liu, X., Aly Saad Aly, M., and Khan, M. Z. H. Electrochemical detection of melamine by using reduced graphene oxide–copper nanoflowers modified glassy carbon electrode. *ACS omega*, 4(23): 20324-20329, 2019.

[66] Lawal, A. T. Recent developments in electrochemical sensors based on graphene for bioanalytical applications. *Sensing and Bio-Sensing Research*, 100571, 2023.

[67] Ghaani, M., Azimzadeh, M., Büyüktaş, D., Carullo, D., and Farris, S. Electrochemical Sensors in the Food Sector: A Review. *Journal of Agricultural and Food Chemistry*, 2024.

[68] Chen, N., Cheng, Y., Li, C., Zhang, C., Zhao, K., and Xian, Y. Determination of melamine in food contact materials using an electrode modified with gold nanoparticles and reduced graphene oxide. *Microchimica Acta*, 182: 1967-1975, 2015.

[69] Begum, I., Ameen, F., Soomro, Z., Shamim, S., AlNadhari, S., Almansob, A., Al-Sabri, A., and Arif, A. Facile fabrication of malonic acid capped silver nanoparticles and their antibacterial activity. *Journal of King Saud University-Science*, 33(1): 101231, 2021.

[70] Shameli, K., Ahmad, M. B., Jazayeri, S. D., Sedaghat, S., Shabanzadeh, P., Jahangirian, H., Mahdavi, M., and Abdollahi, Y. Synthesis and characterization of polyethylene glycol mediated silver nanoparticles by the green method. *International journal of molecular sciences*, 13(6): 6639-6650, 2012.

[71] You, J., Leonard, K., Takahashi, Y., Yonemura, H., and Yamada, S. Effects of silver nanoparticles with different sizes on photochemical responses of polythiophene–fullerene thin films. *Physical Chemistry Chemical Physics*, 16(3): 1166-1173, 2014.

[72] Babu, S. A., and Prabu, H. G. Synthesis of AgNPs using the extract of Calotropis procera flower at room temperature. *Materials Letters*, 65(11): 1675-1677, 2011.

[73] Jayaprakash, N., Vijaya, J. J., Kaviyarasu, K., Kombaiah, K., Kennedy, L. J., Ramalingam, R. J., and Al-Lohedan, H. A. Green synthesis of Ag nanoparticles using Tamarind fruit extract for the antibacterial studies. *Journal of Photochemistry and Photobiology B: Biology*, 169: 178-185, 2017.

[74] Jabbar, A. H., Al-janabi, H. S. O., Hamzah, M. Q., Mezan, S. O., Tumah, A. N., Ameruddin, A. S. B., and Agam, M. A. Green synthesis and characterization of silver nanoparticle (AgNPs) using pandanus atrocarpus extract. *International Journal of Advanced Science Technology*, 29(3): 4913-4922, 2020.

[75] Wang, Y. Electrochemical determination of silver sols for sensor developments, *Doctoral dissertation, University of Bedfordshire*, 2009.

[76] Zhou, Q., Yuan, G., Liu, D., Gu, J., Jiang, S., Xia, Y., and Xiong, W. High efficiency electrochemical degradation of phenol using a Ti/PbO2-Bi-PTh composite electrode. Journal of *The Electrochemical Society*, 167(14): 143506, 2020.

[77] Montes-García, V., Squillaci, M. A., Diez-Castellnou, M., Ong, Q. K., Stellacci, F., and Samori, P. Chemical sensing with Au and Ag nanoparticles. Chemical Society Reviews, 50(2), 1269-1304, 2021.

[78] Chen, X., Hu, Y., Gao, J., Zhang, Y., and Li, S. Interaction of melamine molecules with silver nanoparticles explored by surface-enhanced Raman scattering and density functional theory calculations. *Applied spectroscopy*, 67(5): 491-497, 2013.

[79] Saha, K., Agasti, S. S., Kim, C., Li, X., and Rotello, V. M. Gold nanoparticles in chemical and biological sensing. *Chemical reviews*, 112(5): 2739-2779, 2012.

[80] Mahony, C., Felter, S. P., and McMillan, D. A. An exposure-based risk assessment approach to confirm the safety of hydrogen peroxide for use in home tooth bleaching. *Regulatory Toxicology and Pharmacology*, 44(2): 75-82, 2006.

[81] Arefin, S., Sarker, M. A. H., Islam, M. A., Harun-ur-Rashid, M., and Islam, M. N. Use of Hydrogen Peroxide (H2O2) in raw cow's milk preservation. *Journal of Advanced Veterinary and Animal Research*, 4(4): 371-377, 2017.

[82] Das, S., Goswami, B., and Biswas, K. Milk adulteration and detection: a review. *Sensor letters*, 14(1): 4-18, 2016.

[83] Fakayode, S. O., Lisse, C., Medawala, W., Brady, P. N., Bwambok, D. K., Anum, D., and Grant, C. Fluorescent chemical sensors: applications in analytical, environmental, forensic, pharmaceutical, biological, and biomedical sample measurement, and clinical diagnosis. *Applied Spectroscopy Reviews*, 59(1): 1-89, 2024.

[84] Abd Ali, L. I., Qader, A. F., Salih, M. I., and Aboul-Enein, H. Y. Sensitive spectrofluorometric method for the determination of ascorbic acid in pharmaceutical nutritional supplements using acriflavine as a fluorescence reagent. *Luminescence*, 34(2): 168-174, 2019.

[85] Li, J., Hu, H., Li, H., and Yao, C. Recent developments in electrochemical sensors based on nanomaterials for determining glucose and its byproduct H2O2. *Journal of Materials Science*, 52: 10455-10469, 2017.

[86] Singh, M. Nanosensor platforms for detection of milk adulterants. *Sensors and Actuators Reports*, 5: 100159, 2023.

[87] Motshakeri, M., Sharma, M., Phillips, A. R., and Kilmartin, P. A. Electrochemical methods for the analysis of milk. *Journal of Agricultural and Food Chemistry*, 70(8): 2427-2449, 2022.

[88] Jadon, N., Jain, R., Sharma, S., and Singh, K. Recent trends in electrochemical sensors for multianalyte detection–A review. *Talanta*, 161: 894-916, 2016.

[89] Ghosale, A., Shrivas, K., Deb, M. K., Ganesan, V., Karbhal, I., Bajpai, P. K., and Shankar, R. A low-cost screen-printed glass electrode with silver nano-ink for electrochemical detection of H2O2. *Analytical Methods*, 10(26): 3248-3255, 2018.

[90] Ghosale, A., Shrivas, K., Shankar, R., and Ganesan, V. Low-cost paper electrode fabricated by direct writing with silver nanoparticle-based ink for detection of hydrogen peroxide in wastewater. *Analytical chemistry*, 89(1): 776-782, 2017.

[91] Shrivas, K., Sahu, B., Deb, M. K., Thakur, S. S., Sahu, S., Kurrey, R., ... and Jangde, R. Colorimetric and paper-based detection of lead using PVA capped silver nanoparticles: Experimental and theoretical approach. *Microchemical Journal*, 150: 104156, 2019.

[92] Neog, A., Das, P., and Biswas, R. A novel green approach towards synthesis of silver nanoparticles and it's comparative analysis with conventional methods. *Applied Physics A*, 127(12): 913, 2021.